Journal of the Franklin Institute 362 (2025) 107567

Contents lists available at ScienceDirect

Journal of the Franklin Institute

journal homepage: www.elsevier.com/locate/fi

Frequency analysis of two subsystems coupled by a spring-inerter-damper device and its application to continuous system for vibration control

Jun Wu [a,b], Brano Titurus [a,*]

[a] Department of Aerospace Engineering, University of Bristol, Bristol, UK
[b] Department of Biology, University of Oxford, Oxford, UK

ARTICLE INFO

Keywords:
Spring-inerter-damper device
Two coupled subsystems
Vibration control
Frequency analysis

ABSTRACT

Two continuous subsystems interconnected by a spring-inerter-damper device are common engineering configurations for vibration control. To address the problem of designing device parameters for optimal vibration control, comprehensive and systematic mathematical analyses are carried out for the minimum 2-degrees-of-freedom (DOF) system which includes two subsystems interconnected by a spring-inerter-damper device. Then, the equivalence between the 2DOF system and the full-scale continuous system is established, which allows the results of the 2DOF system to be directly transferrable to the original full-scale system. Results show that there is an optimal tuning condition in which two roots coalesce and both damping ratios reach equally high value at the first bifurcation. The device parameters at this point are derived mathematically, and used for optimal vibration control. The subcritical and supercritical conditions are also defined and the associated properties are derived. When applied to a continuous rotating beam-tendon system as a case study, the device parameters derived based on the equivalent 2DOF system are shown to be close to the optimal parameters with errors less than 6 %, and the performance of the resulting full-scale continuous system is almost identical to the optimal performance.

1. Introduction

Resonant vibration of lightly damped mechanical structures can result in large vibration amplitude or even structural failure in some cases. To suppress the resonant vibration of mechanical systems, traditionally, damping is increased using dampers or other means of passive vibration control. Dampers can be used alone or in combination with springs and inerters. To make dampers work efficiently, a sufficient relative motion between their two ends needs to be retained. Usually, the relative motion between a continuous system and an external fixed point is utilized to activate the damper in stationary structures, e.g., structural dynamics applications. For example, to mitigate vibrations in cable stayed bridges exposed to wind or other excitation sources, a viscous damper [1–6] and an inerter-damper [7] were studied to increase the inherent damping of the stay cables. Another way to generate the required relative motion, applicable to both stationary and moving applications, is to attach a rigid mass at one end of the damper. When combined with elastic restoring elements, this approach leads to the well-known tuned mass damper/absorber concept [8]. Tuned mass dampers have been installed to reduce excessive vibrations in a variety of engineering problems, e.g., the offshore wind turbines [9], rotorcraft blades

* Corresponding author.
E-mail address: Brano.Titurus@bristol.ac.uk (B. Titurus).

https://doi.org/10.1016/j.jfranklin.2025.107567
Received 15 May 2024; Received in revised form 3 December 2024; Accepted 28 January 2025
Available online 29 January 2025

Nomenclature

b_*, k_*	device inertance and stiffness in the optimal tuning condition, respectively
c_{b1}, c_{b2*}	device damping at the first and second bifurcation points in the optimal tuning condition, respectively
Im($*$), Re($*$)	imaginary part and real part of *, respectively
$\mathrm{j} = \sqrt{-1}$	imaginary unit
L	effective length of beam and tendon
P	axial force
w, w_t	transverse displacements of the beam and tendon, respectively
Ω	rotational speed
ζ	damping ratio
ζ_{b1}	damping ratio at the first bifurcation point
ω_∞	circular frequency of the fully locked system
ω'_1, ω'_2	two undamped frequencies in any condition

Subscript

b1, b2	symbols at the first and second bifurcation points, respectively
*	symbols in the optimal tuning condition
$\overline{A}$	conjugate of A

[10–12], beams [13,14], etc. The damper element can also utilize the relative motion between the two flexible structures, e.g., [15–17]. This enables the removal of potentially a very heavy mass element used in the tuned mass absorber configurations. Furthermore, such arrangements are suitable for both stationary and moving dynamic systems. Recently, spring-damper [18] and inerter-damper [19] devices were proposed by the authors to suppress resonant vibrations in the rotorcraft blades via the active tendon concept [20].

Design of the damper-based device (e.g., spring-inerter-damper device or tuned mass damper) aims to achieve optimum vibration control performance. To achieve this, there are mainly three methods of designing the optimal device parameters. In method 1 [21], frequency tuning is based on setting equal magnitude for the dynamic amplification factors at two neutral frequencies (i.e., the frequencies independent of the device damping). The determination of the device damping is based on an average of the device damping that can give a local maximum of the dynamic amplification at each of the two neutral frequencies. In method 2 [22], the frequency tuning is the same as method 1, while the determination of the device damping is based on setting equal dynamic amplification factors at three frequencies, i.e., two neutral frequencies and the fully locked frequency. Applications of method 2 are given in [23,24]. These two methods require the derivation of the analytical form of the dynamic amplification factor, and method 1 also requires the differentiation of the dynamic amplification factor. All these calculations are tedious tasks for higher-order systems. In method 3 [22], the frequency tuning is based on a root-locus diagram obtained by increasing the device damping, in which a bifurcation point emerges as a result of modal interactions. The determination of the device damping is based on finding the bifurcation point in this diagram. All these methods can be directly used on lumped parameter systems. Further, significant attention has been paid recently to the analysis of the lumped parameter 2DOF systems and the impact of the coupling elements interconnecting the two constituent 1DOF blocks on their resultant behaviour, e.g., using spring-inerter-damper device in [25–27], using tuned inerter damper in [24], using inerter-based damper in [28]. When it comes to continuous systems, the direct use of these methods is not possible, and the conversion of the continuous systems to its equivalent lumped parameter systems becomes necessary. However, the expression of the continuous problem in its equivalent reduced order form poses additional difficulty. To this end, Krenk and Høgsberg proposed a quasi-static flexibility correction approach in [23] to compensate for the effect of the higher modes. Later, they also proposed a quasi-dynamic flexibility and inertia correction in [29] to compensate for all non-resonant modes. These corrections have been successfully used in the case of multi-degree-of-freedom systems and one flexible system equipped with damper-based device [23,30]. However, to the best of our knowledge, there are no open publications addressing the problem of how to design the optimal device parameters for the optimal vibration control of two flexible subsystems interconnected by the device.

This work pursues further advancement of active tendon concept [31]. The original motivation was to overcome the problem of the resonant vibration due to insufficient separation between the rotor harmonics and the natural frequencies of rotor blades under the conditions of varying rotor speed. Within this concept, a tendon, which is fixed at the free tip of the blade and passes through the whole blade, is loaded at the root to apply a compressive axial force on the blade. In the early stage, the focus was placed on how the natural frequencies of the blades could be changed with the increasing axial force [32,33] and how to eliminate the tendon-dominated modal frequencies in the considered frequency-loading-speed range [34,35] in both the non-rotating and rotating cases. However, it was found that some blade frequencies were insufficiently sensitive to the axial force; therefore, spring-damper device and inerter-damper devices were introduced to internally connect the beam and tendon in order to increase the damping of these blade modes [18,19]. Such systems involve two flexible subsystems, rotation and varying axial force, complex boundary conditions, among others. This context poses difficulty in designing a suitable spring-damper or inerter-damper device for optimal vibration control.

Motivated by the practical challenges arising during the tuning process of the complex rotating tendon-controlled blade system, this work aims to develop the tuning framework in the reduced order modelling context. The intention is to map the full-scale continuous

system onto an equivalent 2DOF lumped parameter system which permits detailed coupling device tuning via root locus analysis and modal analysis in the complex plane. To this end, this paper addresses the problem of (1) how to design optimal parameters for the spring-inerter-damper device in the minimum 2DOF lumped parameter system to achieve optimal vibration control or mitigation, and (2) how to apply the results of 2DOF system directly to continuous system. Firstly, a generic 2DOF system, where the two constituent parts are interconnected by a spring-inerter-damper device, is put forward and the characteristics of the generic 2DOF system are analysed mathematically while the optimal device parameters for optimal control are derived analytically. Then, the equivalence between the 2DOF system and original continuous systems is established. This allows the results of the 2DOF system analysis to be directly applied to the optimal design of the continuous systems. The framework of this paper is shown in Fig. 1. Building upon the results in this paper, the intended target application is the resonance control of rotorcraft blades using the proposed active tendon concept [36].

The paper is organized as follows: the dynamics of the representative 2DOF system is studied analytically in Section 2. Then, the equivalence between 2DOF system and continuous systems is established and a case study of applying the results of the 2DOF system to the continuous systems is conducted in Section 3. A discussion is provided in Section 4, and the main conclusions are drawn in Section 5.

2. Analysis of a reference 2DOF system

In this section, the objective is to fully analyse the dynamics of the reference 2DOF system analytically. Firstly, the equation of motion is derived in Section 2.1; then the properties in the optimal tuning condition are analysed in Section 2.2. Following this, the subcritical and supercritical parametric conditions are defined and their associated properties are analysed in Section 2.3. Finally, the calculation of the device parameters for the optimal tuning condition is summarized in Section 2.4.

2.1. Equation of motion

The representative reference 2DOF system is interpreted as consisting of two constituent or foundational subsystems, as shown in Fig. 2. One subsystem (left) consists of a rigid body with the mass m_b supported by a spring with the stiffness k_b, while the other subsystem (right) is composed of a rigid body with the mass m_t supported by a spring with the stiffness k_t. These two subsystems are coupled by a spring-inerter-damper device consisting of the stiffness k, inertance b and damping c arranged in parallel. The structural damping of these two subsystems is not considered since the damping ratios of most typical mechanical structures are usually very small (below 0.05).

The equation of motion for the 2DOF system is given by

$$\begin{bmatrix} m_b+b & -b \\ -b & m_t+b \end{bmatrix}\ddot{\mathbf{p}} + \begin{bmatrix} c & -c \\ -c & c \end{bmatrix}\dot{\mathbf{p}} + \begin{bmatrix} k+k_b & -k \\ -k & k+k_t \end{bmatrix}\mathbf{p} = \mathbf{0} \tag{1}$$

where $\mathbf{p} = [x_b \quad x_t]^{\mathrm{T}}$.

By assuming $\mathbf{p} = \mathbf{P}e^{j\omega t}$, where ω is the complex-valued circular frequency, the characteristic equation of Eq. (1) is given by

$$\begin{vmatrix} -\omega^2(m_b+b)+j\omega c+k_b+k & b\omega^2-jc\omega-k \\ b\omega^2-jc\omega-k & -\omega^2(m_t+b)+j\omega c+k_t+k \end{vmatrix} = 0 \tag{2}$$

After simplification, it can be expressed as the polynomial form of ω as follows:

$$\omega^4 + A_3\omega^3 + A_2\omega^2 + A_1\omega + A_0 = 0 \tag{3}$$

where the coefficients are $A_3 = -\frac{(m_b+m_t)jc}{m_bm_t+m_bb+m_tb}$, $A_2 = -\frac{(k+k_b)m_t+k_bb+(k+k_t)m_b+k_tb}{m_bm_t+m_bb+m_tb}$, $A_1 = \frac{(k_b+k_t)jc}{m_bm_t+m_bb+m_tb}$, and $A_0 = \frac{k_bk_t+k_bk+k_tk}{m_bm_t+m_bb+m_tb}$.

When ω is solved, the natural frequency and damping ratio can be derived, respectively, as follows

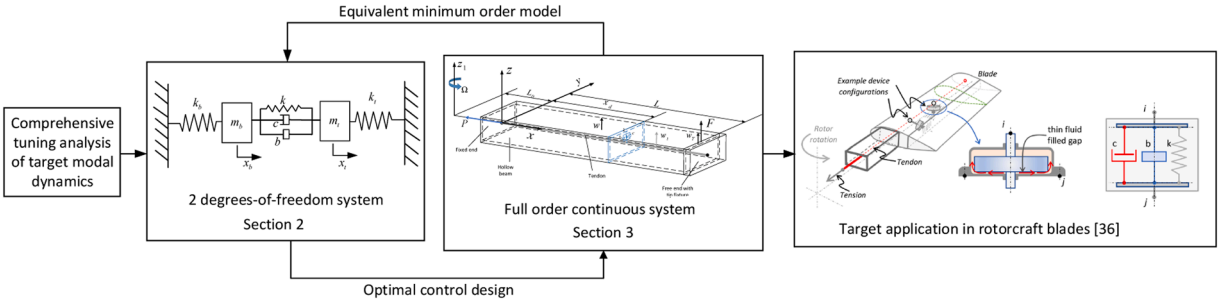

Fig. 1. The framework of this paper.

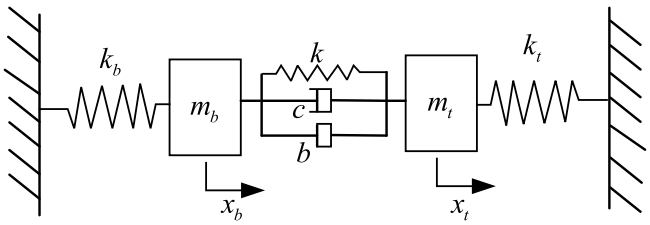

Fig. 2. A representative reference 2DOF system which includes two mass-spring subsystems coupled by a spring-inerter-damper device.

$$f = \frac{|\mathrm{Re}(\omega)|}{2\pi},\ \zeta = \frac{\mathrm{Im}(\omega)}{|\omega|} \tag{4}$$

An exemplary simulation is used to illustrate the characteristics of the system outlined above. The arbitrarily chosen parameters in Table 1 are used for the simulation.

When the inertance b is increased and the stiffness k is kept constant at 100 N/m, the frequency-damping ratio loci linked with the gradual increase in the device damping c can be plotted for several selected inertance levels as shown in Fig. 3. The two shown frequencies originate from two undamped frequencies. One of them ends at the frequency corresponding to the locking induced by the damper, while the other becomes overdamped. It can be seen that there is one branch characterised by the non-localised variation with increasing damping ratio when the device damping c is raised to the infinite value. The other branch is characterised by a localised frequency variation. It also can be noted that there is a critical parametric condition identified by a plane where the two branches intersect. This phenomenon is shown in the green plane (shown in Fig. 4). The relative distribution of the two branches changes when the inertance b passes the critical value.

In Fig. 4, the two undamped frequencies ω'_{1*} and ω'_{2*} are originally located on the real axis. With the increase of device damping c, the frequency loci form a near half-circle. There exists a critical device damping at which these two roots coincide (the first bifurcation point), and then start to bifurcate. With further increase in device damping, one locus goes downward to the fully locked frequency ω_∞, while the other locus proceeds upwards until reaches the second bifurcation point after which the root becomes purely imaginary. Before reaching the second bifurcation, there are two opposite conjugate roots on the left half of the imaginary axis. After the second bifurcation, one root moves upward on the imaginary axis while the other one moves downwards. The characteristics in this plane will be analyzed mathematically in the following sections.

In the same way, when the device stiffness is increased and the device inertance b is kept constant, 2.1 kg chosen here, the frequency-damping ratio loci, with the increasing device damping c, are plotted for several selected stiffness in Fig. 5. Similar phenomenon can be seen there with the increase of the device stiffness k. There is still one branch characterised by the non-local range variation, while the other one is more localised. There is also a critical plane where these two branches intersect (the green plane), which is the same as the green plane in Fig. 4. The two modal branches interchange when the stiffness k passes the critical plane.

2.2. Optimal tuning condition

In the critical plane as shown in Fig. 4, there are two bifurcation points, while there is only one bifurcation point in other planes. To retain clarity, the bifurcation point beyond which two roots are overdamped is called the second bifurcation point consistently in any other plane as well. Therefore, the first bifurcation point only exists in the critical plane.

By observation of Figs. 3 and 5, it can be seen that at the first bifurcation point, the damping ratio is larger than the damping ratio maxima corresponding to the localised loci in any other plane, and the separation between these two frequencies is zero. Hence, this point is selected as the point for optimal tuning and the corresponding plane, as shown in Fig. 4, is named 'optimal tuning plane' in this paper. In the following subsections, the analysis of the properties linked with the optimal tuning condition is developed.

2.2.1. First bifurcation point

In the optimal tuning plane, the four roots are ω_{b1} (double root) and $-\overline{\omega}_{b1}$ (double root) at the first bifurcation point, so the characteristic equation at the first bifurcation point is

$$(\omega - \omega_{b1})^2(\omega + \overline{\omega}_{b1})^2 = 0 \tag{5}$$

It is written in the same form as Eq. (3) as follows:

Table 1
The parameters of the 2DOF system used for the exemplary simulation.

Parameters	Values	Parameters	Values
m_b	9 kg	k_b	1000 N/m
m_t	1 kg	k_t	1000 N/m

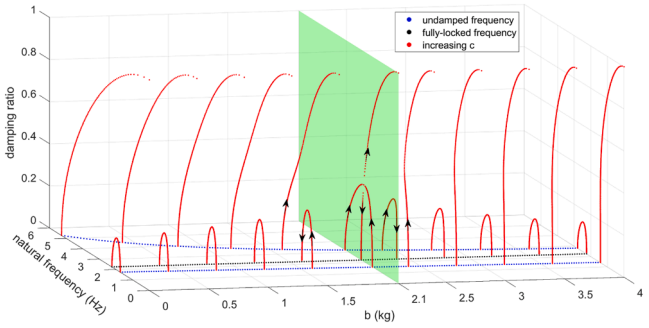

Fig. 3. The variation of the natural frequencies and damping ratios with the increase of the device damping c from 0 to 2000 Ns/m at the selected inertance values. Blue: the variation of the undamped frequencies with the device inertance; black: the variation of the fully locked frequency with the device inertance. The arrows denote the direction of the device damping c increase. The device stiffness k is 100 N/m. The green plane indicates the critical plane.

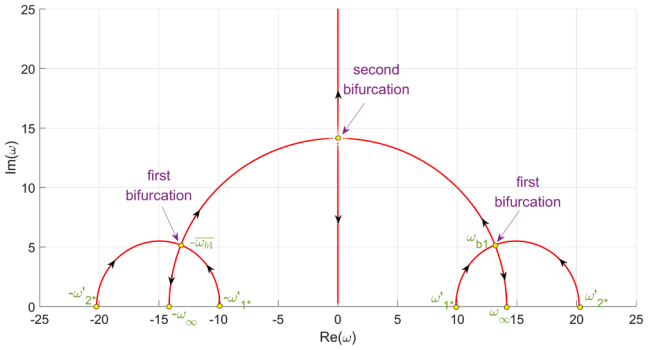

Fig. 4. The complete complex plane root loci obtained when increasing the device damping c in the case of the critical plane (green plane in Fig. 3). The arrows represent the direction of increasing the value of the device damping c parameter.

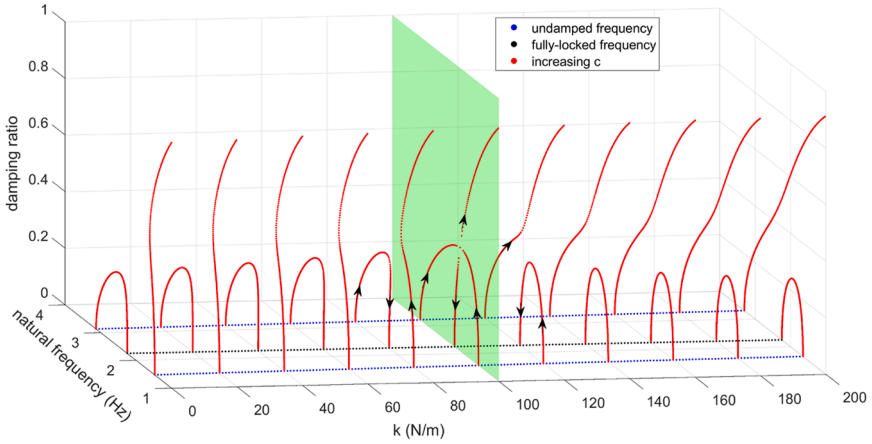

Fig. 5. The variation of the natural frequencies and damping ratios with the increase of the device damping c from 0 to 2000 Ns/m at the selected stiffness. Blue: the variation of the undamped frequency with the device stiffness; black: the variation of the fully locked frequency with the device stiffness. The arrows denote the direction of increasing device damping c. The inertance b is 2.1 kg. The green plane indicates the critical plane.

$$\omega^4 + B_3\omega^3 + B_2\omega^2 + B_1\omega + B_0 = 0 \tag{6}$$

where the coefficients are $B_0 = |\omega_{b1}|^4$, $B_1 = 4\mathrm{jIm}(\omega_{b1})|\omega_{b1}|^2$, $B_2 = -\left[2|\omega_{b1}|^2 + 4\mathrm{Im}(\omega_{b1})^2\right]$, and $B_3 = -4\mathrm{jIm}(\omega_{b1})$.

By equating all the coefficients in Eq. (6) with Eq. (3), four equations are obtained as follows:

$$\text{Linear term}: \ 4\mathrm{jIm}(\omega_{b1})|\omega_{b1}|^2 = \frac{(k_b + k_t)\mathrm{j}c_{b1}}{m_b m_t + m_b b_* + m_t b_*} \tag{7}$$

$$\text{Quadratic term}: \ -\left[2|\omega_{b1}|^2 + 4\mathrm{Im}(\omega_{b1})^2\right] = -\frac{(k_* + k_b)m_t + k_b b_* + (k_* + k_t)m_b + k_t b_*}{m_b m_t + m_b b_* + m_t b_*} = A_{2*} \tag{8}$$

$$\text{Cubic term}: \ -4\mathrm{jIm}(\omega_{b1}) = -\frac{(m_b + m_t)\mathrm{j}c_{b1}}{m_b m_t + m_b b_* + m_t b_*} \tag{9}$$

$$\text{Constant term}: \ |\omega_{b1}|^4 = \frac{k_b k_t + k_b k_* + k_t k_*}{m_b m_t + m_b b_* + m_t b_*} = A_{0*} \tag{10}$$

Dividing the linear term in Eq. (7) by the cubic term in Eq. (9) gives that

$$|\omega_{b1}|^2 = \frac{k_b + k_t}{m_b + m_t} = \omega_\infty^2 \tag{11}$$

where ω_∞ is the circular frequency of the fully locked system, and it is independent of the device inertance and stiffness.

Eq. (11) indicates that the first bifurcation point (ω_{b1}) is located on a circle around the origin with the radius ω_∞.

From Eq. (10), the device inertance and stiffness in the optimal tuning condition satisfy

$$\left(\frac{k_b + k_t}{m_b + m_t}\right)^2 = \omega_\infty^4 = \frac{k_b k_t + k_b k_* + k_t k_*}{m_b m_t + m_b b_* + m_t b_*} \tag{12}$$

If either device stiffness k_* or device inertance b_* is given, the other parameter is only dependent on the masses and stiffness of two subsystems. This equation is used to determine the device inertance or stiffness in the optimal tuning condition.

2.2.2. Undamped system

For any device inertance b and device stiffness k, the characteristic equation for the undamped system is derived by setting device damping c in Eq. (3) to zero as follows:

$$\omega^4 + C_2\omega^2 + C_0 = 0 \tag{13}$$

where the coefficients are $C_2 = -\frac{(k+k_b)m_t + k_b b + (k+k_t)m_b + k_t b}{m_b m_t + m_b b + m_t b}$, and $C_0 = \frac{k_b k_t + k_b k + k_t k}{m_b m_t + m_b b + m_t b}$.

When $b = b_*$ and $k = k_*$ (in the optimal tuning condition), it can be derived from Eqs. (3) and (13) that

$$\omega'^2_{1*} + \omega'^2_{2*} = -C_{2*} = -A_{2*} \tag{14}$$

$$\omega'^2_{1*}\omega'^2_{2*} = C_{0*} = A_{0*} \tag{15}$$

where ω'_{1*} and ω'_{2*} are the two undamped frequencies in the optimal tuning condition. It is further assumed that $\omega'_{1*} < \omega'_{2*}$.

From Eqs. (10) and (15), it can be derived that

$$\omega'_{1*}\omega'_{2*} = |\omega_{b1}|^2 = \omega_\infty^2 \tag{16}$$

It can be derived from Eq. (8) that

$$2\omega'_{1*}\omega'_{2*} + 4\zeta_{b1}^2|\omega_{b1}|^2 = \omega'^2_{1*} + \omega'^2_{2*} \tag{17}$$

where ζ_{b1} is the damping ratio at the first bifurcation point, which is derived from Eq. (17) as follows:

$$\zeta_{b1} = \frac{\omega'_{2*} - \omega'_{1*}}{2\omega_\infty} = \frac{\omega'_{2*} - \omega'_{1*}}{2\sqrt{\omega'_{2*}\omega'_{1*}}} = \frac{\sqrt{-A_{2*} - 2\omega_\infty^2}}{2\omega_\infty} \tag{18}$$

where the right hand side term is derived from Eqs. (14), (16).

Knowing any two of these three frequencies (ω'_{1*}, ω'_{2*} and ω_∞), the damping ratio at the first bifurcation point can be derived. To get a higher damping ratio at the first bifurcation point, larger separation between ω'_{2*} and ω'_{1*} is required. It can also be derived by first calculating A_{2*} from Eq. (8) and then substituting into Eq. (18).

The imaginary part of the root at the first bifurcation point is given by

$$\mathrm{Im}(\omega_{b1}) = \zeta_{b1}|\omega_{b1}| = \frac{\omega'_{2*} - \omega'_{1*}}{2} \tag{19}$$

After substituting Eq. (19) into Eq. (9), the device damping at the first bifurcation point is derived as follows:

$$c_{b1} = 4\zeta_{b1}\omega_\infty \frac{m_b m_t + m_b b_* + m_t b_*}{m_b + m_t} \tag{20}$$

It can be seen that c_{b1} is dependent on b_* and k_* (the relationship between b_* and k_* shown in Eq. (12)), so the device inertance b and device stiffness k determine the tuning condition/plane (as shown in Eq. (12)), while the device damping c does not, but only determines where the four roots are located in the determined tuning plane.

2.2.3. Damping ratio at the first bifurcation

It is of interest to see how the system parameters and the spring-inerter-damper device influence the critical damping ratio at the first bifurcation point. According to Eq. (12), increasing k_* is equivalent to increasing b_* to reach the optimal tuning condition, and vice versa. In this section, the influence of the varying b_* on the critical damping ratio is studied. The obtained conclusion is also applicable to varying k_*.

It can be derived from Eqs. (14), (15) that

$$\omega'^2_{2*} = \frac{-C_{2*} + \sqrt{C_{2*}^2 - 4\omega_\infty^4}}{2} \tag{21}$$

Substituting k_* solved from Eq. (12) into $-C_{2*}$ below Eq. (13) gives

$$-C_{2*} = \omega_\infty^2 + \frac{(k_b + k_t)^2 b_* + k_b^2 m_t + k_t^2 m_b}{(m_b + m_t)(k_b + k_t)b_* + m_b m_t (k_b + k_t)} \tag{22}$$

It can be directly shown that $-C_{2*}$ decreases monotonically with increasing b_*. If b_* is increased, $-C_{2*}$ decreases, then ω'_{2*} decreases according to Eq. (21), and ω'_{1*} increases according to Eq. (16), so the damping ratio at the first bifurcation ζ_{b1} decreases according to Eq. (18). In the same way, it can be proven that the increase in k_* leads to the decrease of ζ_{b1} since increasing k_* is equivalent to increasing b_*. It means the increase of device inertance or device stiffness restrains the increase of the damping ratio at the first bifurcation for optimal tuning.

2.2.4. Characteristics before second bifurcation

For any b and k (in any plane), the four roots are ω_1, ω_2, $-\overline{\omega}_1$, $-\overline{\omega}_2$ before the system reaches the second bifurcation, and the characteristic equation in this case is

$$(\omega - \omega_1)(\omega - \omega_2)(\omega + \overline{\omega}_1)(\omega + \overline{\omega}_2) = 0 \tag{23}$$

It is written in the same form as Eq. (3) as follows

$$\omega^4 + D_3\omega^3 + D_2\omega^2 + D_1\omega + D_0 = 0 \tag{24}$$

where the coefficients are $D_3 = -2\mathrm{j}(\zeta_1|\omega_1| + \zeta_2|\omega_2|)$, $D_2 = -4\zeta_1\zeta_2|\omega_1||\omega_2| - |\omega_1|^2 - |\omega_2|^2$, $D_1 = 2\mathrm{j}\left(\zeta_1|\omega_2|^2|\omega_1| + \zeta_2|\omega_1|^2|\omega_2|\right)$ and $D_0 = |\omega_1|^2|\omega_2|^2$.

These coefficients can be equated with those in Eq. (3). It can be derived that

$$\frac{D_1}{D_3} = -\frac{\zeta_1|\omega_2|^2|\omega_1| + \zeta_2|\omega_1|^2|\omega_2|}{\zeta_1|\omega_1| + \zeta_2|\omega_2|} = \frac{A_1}{A_3} = -\omega_\infty^2 \tag{25}$$

If in the optimal tuning condition ($b = b_*$ and $k = k_*$), equating D_0 with A_{0*} in Eq. (10) gives

$$|\omega_1||\omega_2| = |\omega_{b1}|^2 = \omega_\infty^2 \tag{26}$$

Then, it can be derived from Eq. (25) that

$$(|\omega_1| - |\omega_2|)(\zeta_1 - \zeta_2) = 0 \tag{27}$$

According to Eqs. (26), (27), the following two scenarios are considered:

(1) $c_{b1} \le c \le c_{b2*}$ (the system between the first and second bifurcation), where c_{b2*} is the device damping at the second bifurcation

Considering Fig. 4, it can be derived from Eq. (27) that

$$|\omega_1| = |\omega_2| = \omega_\infty \tag{28}$$

This means the all four roots are on the circle of radius ω_∞. Equating D_2 with A_{2*} in Eq. (8) gives that

$$-4\zeta_1\zeta_2|\omega_1||\omega_2| - |\omega_1|^2 - |\omega_2|^2 = -\left(\omega'^2_{1*} + \omega'^2_{2*}\right) \tag{29}$$

Then using Eqs. (16), (18), (28), (29), a relationship between their damping ratios is derived as

$$\zeta_1\zeta_2 = \left(\frac{\omega'_{2*} - \omega'_{1*}}{2\omega_\infty}\right)^2 = \zeta_{b1}^2 \tag{30}$$

Eq. (30) means that the multiplication of the damping ratios of two roots on the same side is a constant ζ_{b1}^2.

(2) $c \le c_{b1}$ (the system before the first bifurcation)

Considering Fig. 4, it can be derived from Eq. (27) that

$$\zeta_1 = \zeta_2 = \widetilde{\zeta} \tag{31}$$

This means that the damping ratios of all four roots are the same.
Considering Eq. (26), it can be derived that

$$\omega_1\overline{\omega}_2 = \overline{\omega}_1\omega_2 = \omega_\infty^2 \tag{32}$$

From this, the four roots are ω_i, $\omega_\infty^2/\overline{\omega}_i$, $-\overline{\omega}_i$, $-\omega_\infty^2/\omega_i$ ($i = 1$ or 2).
This also means that before reaching the first bifurcation, the two angles formed between the lines connecting the roots and the origin with the real axis are the same when changing the device damping c. Further, there is a fixed relationship between their moduli as implied by Eq. (26), i.e., the multiplication of the moduli of two roots on the same side is a constant ω_∞^2.
Then, it can be further derived from Eq. (29) that

$$4\omega_\infty^2\widetilde{\zeta}^2 + |\widehat{\omega}|^2 + \frac{\omega_\infty^4}{|\widehat{\omega}|^2} = \omega'^2_{1*} + \omega'^2_{2*} \tag{33}$$

where $\widehat{\omega}$ can be either ω_1 or ω_2.

Eq. (33) suggests that there is a fixed relationship between $\widetilde{\zeta}$ and $|\widehat{\omega}|$. After explicitly introducing the real and imaginary parts for $\widehat{\omega}$, the relationship between them can be written as follows

$$\begin{aligned}&\mathrm{Im}(\widehat{\omega})^4 + \mathrm{Re}(\widehat{\omega})^4 + 2\mathrm{Im}(\widehat{\omega})^2\mathrm{Re}(\widehat{\omega})^2 + \left(4\omega'_{1*}\omega'_{2*} - \omega'^2_{1*} - \omega'^2_{2*}\right)\mathrm{Im}(\widehat{\omega})^2\\ &-\left(\omega'^2_{1*} + \omega'^2_{2*}\right)\mathrm{Re}(\widehat{\omega})^2 + \omega'^2_{1*}\omega'^2_{2*} = 0\end{aligned} \tag{34}$$

This means the mapping $\left(\underbrace{\mathrm{Im}(\widehat{\omega})^2}_{x}, \underbrace{\mathrm{Re}(\widehat{\omega})^2}_{y}\right)$ of the points $(\mathrm{Im}(\widehat{\omega}), \mathrm{Re}(\widehat{\omega}))$ belonging to the root trajectory forms a parabola characterised by the following expression

$$x^2 + y^2 + 2xy + \left(4\omega'_{1*}\omega'_{2*} - \omega'^2_{1*} - \omega'^2_{2*}\right)x - \left(\omega'^2_{1*} + \omega'^2_{2*}\right)y + \omega'^2_{1*}\omega'^2_{2*} = 0 \tag{35}$$

Eq. (35) gives the mathematical expression for the half-circle-like locus before the first bifurcation, as shown in Fig. 4.

2.2.5. *Characteristics after second bifurcation*

After the second bifurcation, two roots become purely imaginary (overdamped). For any b and k (in any plane), there is a pair of complex roots ω_1 and $-\overline{\omega}_1$, and two purely imaginary roots $\omega_2 = \mathrm{j}|\omega_2|$ and $\omega_3 = \mathrm{j}|\omega_3|$ after the system reaches the second bifurcation point. It is assumed that $|\omega_2| \le |\omega_3|$. The characteristic equation in this case is

$$(\omega - \omega_1)(\omega + \overline{\omega}_1)(\omega - \omega_2)(\omega - \omega_3) = 0 \tag{36}$$

It is written in the same form as Eq. (3) as follows

$$\omega^4 + E_3\omega^3 + E_2\omega^2 + E_1\omega + E_0 = 0 \tag{37}$$

where the coefficients are $E_3 = -\mathrm{j}(2\mathrm{Im}(\omega_1) + |\omega_2| + |\omega_3|)$, $E_2 = -|\omega_2||\omega_3| - |\omega_1|^2 - 2\mathrm{Im}(\omega_1)(|\omega_2| + |\omega_3|)$, $E_1 = \mathrm{j}\left(|\omega_1|^2(|\omega_2| + |\omega_3|) + 2\mathrm{Im}(\omega_1)|\omega_2\|\omega_3|\right)$ and $E_0 = |\omega_1|^2|\omega_2\|\omega_3|$.

Using the relation $\frac{A_1}{A_3} = -\omega_\infty^2 = \frac{E_1}{E_3}$ (refer to Eq. (25)) gives

$$2\mathrm{Im}(\omega_1)\left(|\omega_2||\omega_3| - \omega_\infty^2\right) + (|\omega_2| + |\omega_3|)\left(|\omega_1|^2 - \omega_\infty^2\right) = 0 \tag{38}$$

If in the optimal tuning condition ($b = b_*$ and $k = k_*$), equating E_0 with A_{0*} and equating E_2 with A_{2*}, respectively, give

$$|\omega_1|^2|\omega_2||\omega_3| = \omega_\infty^4 \tag{39}$$

$$|\omega_2||\omega_3| + |\omega_1|^2 + 2\mathrm{Im}(\omega_1)(|\omega_2| + |\omega_3|) = \omega'^2_{1*} + \omega'^2_{2*} = 2\omega_\infty^2 + 4\zeta_{b1}^2\omega_\infty^2 \tag{40}$$

Combining Eqs. (38), (39) gives

$$\left(\omega_\infty^2 - |\omega_1|^2\right)\left[2\mathrm{Im}(\omega_1)\omega_\infty^2 - (|\omega_2| + |\omega_3|)|\omega_1|^2\right] = 0 \tag{41}$$

It can be obtained from Eq. (41) that

$$|\omega_1| = \omega_\infty \tag{42}$$

This means after the second bifurcation in the optimal tuning condition, the pair of complex roots is still on the circle of radius ω_∞. Then, it can be derived from Eq. (39) that

$$|\omega_2||\omega_3| = \omega_\infty^2 \tag{43}$$

This means the multiplication of the moduli of the two purely imaginary roots is a constant ω_∞^2. With the assumption of $|\omega_2| \le |\omega_3|$, then $|\omega_3| \ge \omega_\infty \ge |\omega_2|$. Thus, the two purely imaginary roots are always separated by the fully locked frequency ω_∞.

Combining Eqs. (40), (42), (43) gives the damping ratio of the pair of complex roots as follows:

$$\zeta_{\omega_1} = \frac{\mathrm{Im}(\omega_1)}{|\omega_1|} = \frac{2\zeta_{b1}^2\omega_\infty}{\frac{\omega_\infty^2}{|\omega_3|} + |\omega_3|} \tag{44}$$

Thus, if $|\omega_3|$ is increased, then $|\omega_2|$ is reduced, and ζ_{ω_1} is reduced, and vice versa.

At the second bifurcation point, the two purely imaginary roots are $(\omega_2)_{b2*} = \mathrm{j}\omega_\infty$ and $(\omega_3)_{b2*} = \mathrm{j}\omega_\infty$, and their damping ratio is 1. Eq. (30) is still satisfied, so the damping ratio of the pair of complex roots ($(\omega_1)_{b2*}$ and $-(\overline{\omega}_1)_{b2*}$) can be obtained as

$$(\zeta_{\omega_1})_{b2*} = \frac{\mathrm{Im}((\omega_1)_{b2*})}{\omega_\infty} = \zeta_{b1}^2 \tag{45}$$

where the subscript b2* means the value at the second bifurcation in the optimal tuning condition.

Additionally, equating E_3 with A_3 gives

$$2\mathrm{Im}((\omega_1)_{b2*}) + 2\omega_\infty = \frac{(m_b + m_t)c_{b2*}}{m_b m_t + m_b b_* + m_t b_*} \tag{46}$$

Using Eqs. (45), (46), the device damping (c_{b2*}) at the second bifurcation point in the optimal tuning condition (plane) is derived as

$$c_{b2*} = \frac{2\omega_\infty\left(\zeta_{b1}^2 + 1\right)(m_b m_t + m_b b_* + m_t b_*)}{m_b + m_t} \tag{47}$$

2.2.6. *Example*

To visualise the variation of the four roots with increasing device damping c in the optimal tuning plane, their moduli and damping ratios, for the previous chosen illustration parameter set, are plotted in Fig. 6. The corresponding complete complex plane frequency loci are plotted in Fig. 4. Before the first bifurcation ($c<c_{b1}$), the damping ratios of the four roots are the same (Eq. (31)) and keep increasing with the increasing device damping c, while their moduli satisfy Eq. (26), so their moduli are symmetric about ω_∞ when plotted in the log scale. Between the first and second bifurcation ($c_{b1}<c<c_{b2*}$), the moduli of the four roots are the same and keep constant with the increasing device damping c (Eq. (28)), while the damping ratios satisfy Eq. (30). This is why the damping ratios are symmetric about ζ_{b1} when plotted in the log scale. After the second bifurcation ($c>c_{b2*}$), two roots become purely imaginary, so their

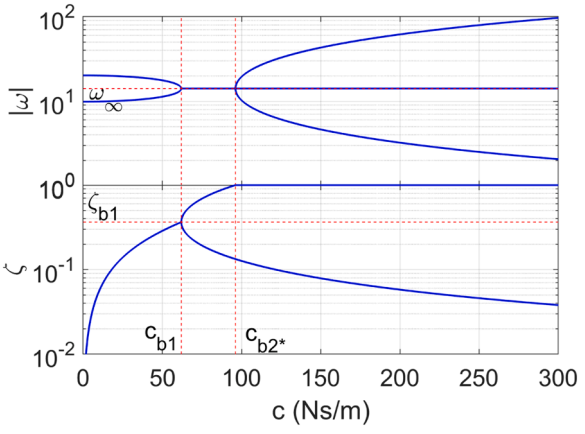

Fig. 6. The variation of the moduli and damping ratios of the four roots with increasing device damping c in the optimal tuning plane. The corresponding complete complex plane frequency loci are plotted in Fig. 4.

damping ratios are 1. Their moduli satisfy Eq. (43), which explains their symmetry about ω_∞ when plotted in the log scale. The other two complex roots are still on the circle of radius ω_∞ (Eq. (42)), while their damping ratios given by Eq. (44) keep decreasing with the increasing device damping c until reaching 0, where the system is fully locked by the infinite device damping.

2.3. Subcritical and supercritical tuning conditions

This section discusses the properties in the planes that do not correspond to the optimal tuning conditions. To classify these conditions, a function is defined using the two undamped frequencies ω'_1 and ω'_2 and the fully-locked frequency ω_∞ as

$$h = \omega_\infty^2 - \omega'_1\omega'_2 \tag{48}$$

With this definition, $h = 0$ indicates the optimal tuning condition according to Eq. (16). The planes satisfying the condition $h < 0$ are defined as the subcritical planes, while those satisfying the condition $h > 0$ are defined as the supercritical planes.

2.3.1. Varying inertance b

When the device stiffness $k = k_*$ is fixed, while the device inertance b is changing. It can be divided into two cases: (1) $b < b_*$; (2) $b > b_*$.

2.3.1.1. Case $b < b_*$. Before the second bifurcation, when $b < b_*$, $D_0 = |\omega_1|^2|\omega_2|^2 = A_0 > A_{0*} = \omega_\infty^4$ (the right hand side results from Eqs. (10), (11)), so the two undamped frequencies and the fully locked frequency satisfy the following condition

$$h = \omega_\infty^2 - \omega'_1\omega'_2 < 0 \tag{49}$$

This means the corresponding plane is a subcritical plane. It can be derived from Eq. (25) that

$$|\omega_1||\omega_2|(|\omega_1| - |\omega_2|)(\zeta_1 - \zeta_2) > 0 \tag{50}$$

Assume $|\omega_2| > |\omega_1|$, then $\zeta_2 > \zeta_1$; and vice versa. This means the root with larger modulus has larger damping ratio before the second bifurcation.

The loci of the imaginary versus real parts of the roots, in the case of device inertance being 0.8 kg and stiffness being 100 N/m, are plotted in Fig. 7(a). The device inertance is smaller than the critical inertance of 2.1 kg, so it belongs to subcritical condition. The locally evolving or, simply, local loci are encompassed by the non-local loci. It can be seen from Fig. 7(b) that before the second bifurcation, the non-local loci have larger moduli and higher damping ratios than the local loci under the same device damping, which is consistent with Eq. (50); after the second bifurcation, one branch of the non-local loci increases while the other moves down on the imaginary axis; and their damping ratios are 1. At the same time, the local loci converge to the fully locked state with the damping ratios dropping to zero and moduli increasing towards the fully locked frequency.

2.3.1.2. Case $b > b_*$. In the same way, when $b > b_*$, because $D_0 = |\omega_1|^2|\omega_2|^2 = A_0 < A_{0*} = \omega_\infty^4$ (the right hand side results from Eqs. (10), (11)), the two undamped frequencies and the fully locked frequency satisfy the following conditions

$$h = \omega_\infty^2 - \omega'_1\omega'_2 > 0 \tag{51}$$

$$|\omega_1||\omega_2|(|\omega_1| - |\omega_2|)(\zeta_1 - \zeta_2) < 0 \tag{52}$$

The corresponding plane is a supercritical plane. Assume $|\omega_2| > |\omega_1|$, then $\zeta_2 < \zeta_1$; and vice versa. This means the root with larger

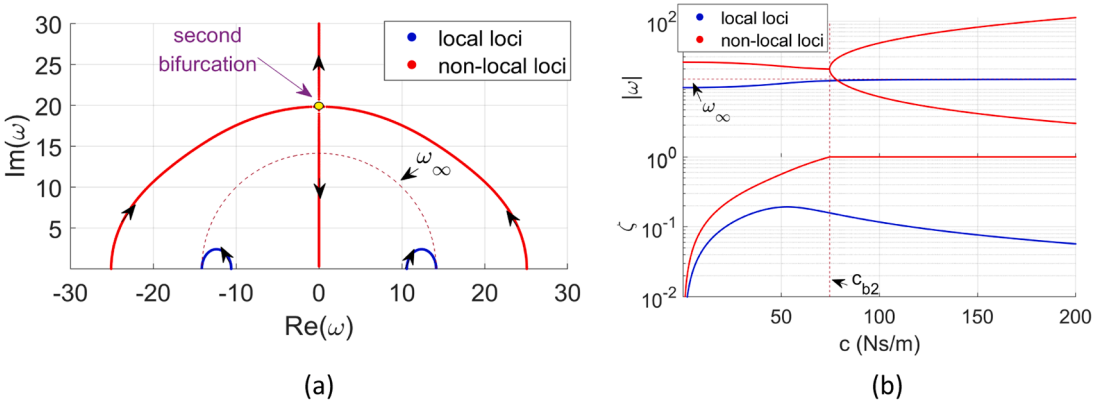

Fig. 7. (a) The loci of the imaginary versus real parts of the roots; (b) the variation of the moduli and damping ratios of the roots with increasing device damping c when the device inertance is 0.8 kg and stiffness is 100 N/m (subcritical plane). The arrows in (a) indicate the direction of increasing device damping.

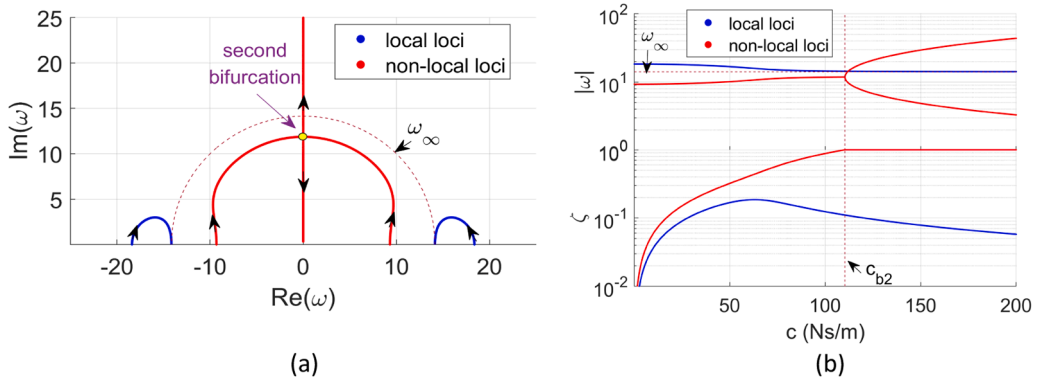

Fig. 8. (a) The loci of the imaginary versus real parts of the roots; (b) the variation of the moduli and damping ratios of the roots with increasing device damping c when the device inertance is 3.2 kg and stiffness is 100 N/m (supercritical plane). The arrows in (a) indicate the direction of increasing device damping.

modulus has smaller damping ratio before the second bifurcation.

The loci of the imaginary versus real parts of the roots, in the case of the device inertance being 3.2 kg and stiffness being 100 N/m, are plotted in Fig. 8(a). The device inertance is larger than the critical inertance of 2.1 kg, so it belongs to supercritical condition. The local loci are located outside the non-local loci. It can be seen from Fig. 8(b) that before the second bifurcation, the non-local loci have smaller moduli and higher damping ratios than the local loci under the same device damping, which is consistent with Eq. (52). After the second bifurcation, one branch of the non-local loci raises up while the other moves down on the imaginary axis, and their damping ratios are 1. At the same time, the local loci converge to the fully locked state with the damping ratios dropping to zero and moduli decreasing to the fully locked frequency.

It can be seen that with the increase of the device inertance, the system undergoes transformation from a subcritical to a supercritical parametric condition.

2.3.2. *Varying stiffness k*

When the inertance $b = b_*$ is fixed, while the device stiffness k is changed. It can be divided into two cases: (1) $k < k_*$; (2) $k > k_*$.

2.3.2.1. Case $k < k_*$. The case of $k < k_*$ is qualitatively equivalent to the case of $b > b_*$ in Section 2.3.1. Therefore, the corresponding plane is a supercritical plane. The properties of the four roots with increasing device damping will be similar to those in Fig. 8.

2.3.2.2. Case $k > k_*$. The case of $k > k_*$ is qualitatively equivalent to the case of $b < b_*$ in Section 2.3.1. Therefore, the corresponding plane is a subcritical plane. The properties of the four roots with increasing device damping will be similar to those in Fig. 7.

With the increase of the device stiffness, the system undergoes transformation from a supercritical condition to a subcritical parametric condition.

2.3.3. *Some properties in the subcritical and supercritical tuning conditions*

Property 1. *The non-local and local trajectories will never cross in the subcritical and supercritical planes.*

The two inequalities Eqs. (50) and (52) indicate the non-local and local root trajectories will never cross before the second bifurcation in the subcritical and supercritical planes. After the second bifurcation, the two non-local loci are located on the imaginary axis, while the two local loci are still complex-valued and tend to converge to the real-valued roots with the increasing device damping. Thus, this proves that the non-local and local trajectories will never cross in the subcritical and supercritical planes.

Property 2. *The loci with larger undamped frequency is non-local in the subcritical plane, while the loci with smaller undamped frequency is non-local in the supercritical plane.*

It is also indicated by Eqs. (50) and (52) that neither the damping ratios nor the moduli corresponding to the non-local and local loci will be equal before the second bifurcation in the subcritical and supercritical planes. Considering that the roots (including the modulus and damping ratio) corresponding to the non-local and local loci are continuous with the varying device damping, the non-local loci always have the higher damping ratio since its damping ratio is equal to 1 at the second bifurcation. In the subcritical plane, the non-local loci always have larger moduli than the local loci before the second bifurcation since the roots with larger moduli have larger damping ratios. In contrast, the non-local loci always have smaller moduli in the supercritical plane before the second bifurcation. This proves the loci with larger undamped frequency is non-local in the subcritical plane, while the loci with smaller undamped frequency is non-local in the supercritical plane.

Property 3. *The local and non-local trajectories are always separated by the fully locked frequency before the second bifurcation in both the*

subcritical and supercritical planes.

In the subcritical plane, the roots with smaller moduli corresponds to the local loci, and the moduli keep increasing until they converge to the fully locked frequency, so the moduli satisfy $|\omega_1| < \omega_\infty$ before the second bifurcation. Given that $|\omega_1 \| \omega_2| > \omega_\infty^2$ before the second bifurcation, the other moduli corresponding to the non-local loci must satisfy $|\omega_2| > \omega_\infty$. In the supercritical plane, the roots with larger moduli corresponds to local loci, and the moduli keep decreasing until they converge to the fully locked frequency, so the moduli satisfy $|\omega_2| > \omega_\infty$ before the second bifurcation. Given that $|\omega_1 \| \omega_2| < \omega_\infty^2$ before the second bifurcation, the other moduli corresponding to the non-local loci must satisfy $|\omega_1| < \omega_\infty$. To summarize, in both the subcritical and supercritical planes, the moduli of the roots always satisfy $|\omega_1| < \omega_\infty < |\omega_2|$ before the second bifurcation. This means that the local and non-local trajectories are always separated by the fully locked frequency before the second bifurcation in both the subcritical and supercritical planes, just as shown in Figs. 7(a) and 8(a).

2.4. Summary

When the mass and stiffness of the two subsystems are known, the coupling device parameters for the optimal tuning of the 2DOF system shown in Fig. 2 can be determined directly according to Table 2. These parameters can be used as a guide when designing optimally tuned vibration control configuration of a mechanical system of choice.

When designing the device, either device inertance or device stiffness should be given, and Eq. (12) is used to calculate the other in the optimal tuning condition. Then the fully locked frequency ω_∞ is calculated using Eq. (11). Then A_{2*} is calculated using Eq. (8), and the damping ratio at the first bifurcation point ζ_{b1} is calculated using Eq. (18) with the calculated A_{2*}; the device damping at the first bifurcation point c_{b1} is calculated using Eq. (20) with the calculated ζ_{b1}; Then the device damping at the second bifurcation point c_{b2*} is calculated using Eq. (47) with the calculated ζ_{b1}.

3. Application to a continuous system

The results of the 2DOF system analysis can be applied to the case involving two coupled continuous systems. Initially, however, an appropriate procedure needs to be used to transform the original continuous system to its reduced order and equivalent 2DOF form. A case involving a rotating beam-tendon system is used as an example to illustrate this process. The rotating beam-tendon system originates from the active tendon concept [18,19,34], which was proposed to control the resonant vibration of helicopter blades by applying an axial force using a tendon. In this configuration, the beam is used to simulate the helicopter blade. The axial force can change the frequencies of the beam-dominated modes when they are close to the rotor harmonics, so the resonant vibration can be avoided at different rotational speeds. However, it was found that some of the beam-dominated modes were not sensitive to the axial force, which compromises the idea of changing their frequencies by applying the axial force. To address this limitation, the guiding spring-inerter-damper device was proposed to link the beam and tendon to increase the damping of the beam-dominated modes through the relative motion between the beam and tendon. The aim of this section is to show how the results of the 2DOF analysis can be used for designing the optimal parameters of the coupling device in continuous systems. In the following subsections, firstly, a procedure for establishing the equivalence between the rotating beam-tendon continuous system and the minimum 2DOF system is introduced. Then, a case study is conducted to illustrate how to use the results of the 2DOF system analysis to optimally increase the damping of the beam-dominated modes. However, it should be noted that when reducing the continuous system to its equivalent 2DOF system, the two subsystems in the 2DOF system represent the two modes of interest of the continuous system, i.e., one mode dominated by the beam activity and one mode dominated by the tendon activity. They do not correspond to the two constituent physical subsystems, i.e., beam and tendon.

3.1. Equivalence

3.1.1. Model description

The rotating beam-tendon model developed in a previous paper [19] is used here, as shown in Fig. 9. The choice of this model is made because it was validated against the experiment in [18] and against a finite element model in [19]. Note that the beam-tendon system is only used as a conceptual case, but not the target application. The target application is the rotorcraft blade-tendon system, as shown in Fig. 1. The beam is a cantilever beam with hollow rectangular cross-section, while the tendon passes through the whole body

Table 2
Summary of the formulae in the optimal tuning condition.

Parameters	Calculation
Device inertance b_* or stiffness k_*	Eq. (12)
Device damping at the first bifurcation point c_{b1}	Eq. (20)
Damping ratio at the first bifurcation point ζ_{b1}	Eqs. (8), (18)
Device damping at the second bifurcation point c_{b2*}	Eq. (47)

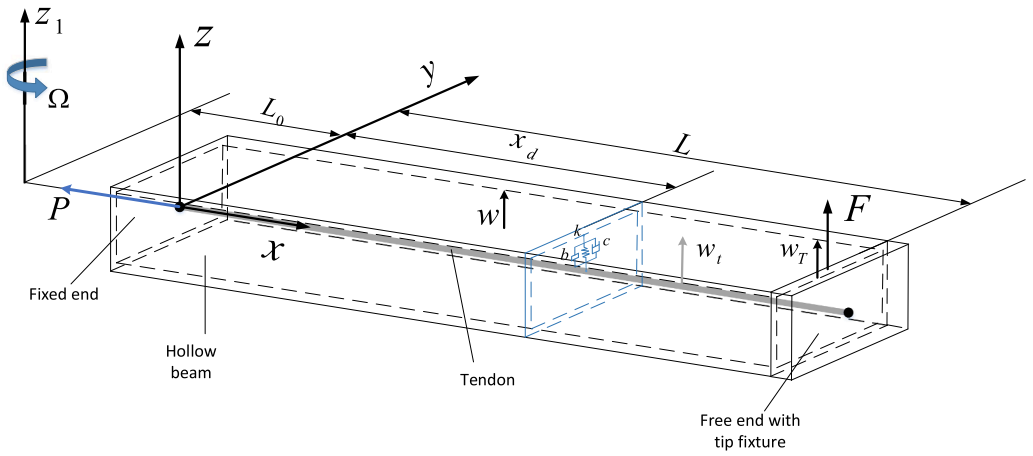

Fig. 9. The rotating beam-tendon model interconnected by a spring-inerter-damper device at the location of x_d.

of the beam and is coincident with the elastic axis of the beam in the undeformed position. The beam and tendon are both fixed at the left end, while they are free at the right end but connected with each other by a rigid tip fixture. Both the beam and tendon have an effective length of L. The tendon is loaded with a constant tension P that acts as a compressive axial force applied to the beam. The beam-tendon system is rotating with a constant rotational speed of Ω about the z_1 axis, which has an offset of L_0 from the fixed end of the beam. Only the transverse deflections of the beam $w(x,t)$ and the tendon $w_t(x,t)$ are considered. The tip fixture has a transverse displacement w_T. Further, the beam and tendon are connected transversely using a spring-inerter-damper device at the location of x_d. The stiffness, inertance and damping of the device are k, b and c, respectively. To be consistent with the no-damping situation in the 2DOF system, the structural damping of the primary beam-tendon system is not considered. Furthermore, the structural damping ratio is usually very small (<0.05), so it is expected that the damping will not influence the dynamics significantly.

3.1.2. *Equivalent parameters*

The beam is modelled as a Timoshenko beam with the consideration of transverse displacement and cross-sectional rotation, while the tendon is modelled as a string with the consideration of its transverse displacement. According to [19], the equation of motion for the rotating beam-tendon system is given by

$$\mathbf{M}\ddot{\mathbf{q}} + \mathbf{K}\mathbf{q} = \mathbf{f} \tag{53}$$

where $\mathbf{q} = [\,\mathbf{q}_z \quad \mathbf{q}_r \quad \mathbf{q}_{tz} \quad w_T\,]$ is the full generalized coordinate vector of the system, in which $\mathbf{q}_z$, $\mathbf{q}_r$ and $\mathbf{q}_{tz}$ are the generalized coordinate vectors of the transverse displacement of the beam, cross-sectional rotational angle of the beam, and the transverse displacement of the tendon, respectively; $\mathbf{M} = \mathrm{diag}(\,\mathbf{M}_b \quad \mathbf{M}_t \quad m_T\,)$ is the mass matrix, in which $\mathbf{M}_b$ and $\mathbf{M}_t$ are the mass matrices of the beam and tendon, respectively, and m_T is the mass of the tip fixture; $\mathbf{K} = \mathrm{diag}\big(\,\mathbf{K}_{b1} + \mathbf{K}_{b2} + \Omega^2\mathbf{K}_{b3} - \Omega^2\mathbf{K}_{b4} - P\mathbf{K}_{bP} \quad \Omega^2\mathbf{K}_{t3} + P\mathbf{K}_{tP} \quad 0\,\big) + \mathbf{K}_c$ is the stiffness matrix, in which $\mathbf{K}_{b1}$, $\mathbf{K}_{b2}$, $\mathbf{K}_{b3}$, $\mathbf{K}_{b4}$ and $\mathbf{K}_{bP}$ are the stiffness matrices of the beam due to flexural deflection, shear deflection, centrifugal effect, the velocity in the rotational plane arising from the deformation caused by the beam cross-sectional rotation and the applied axial force, respectively; $\mathbf{K}_{t3}$ and $\mathbf{K}_{tP}$ are the stiffness matrices of the tendon due to centrifugal effect and applied axial force, respectively; $\mathbf{K}_c$ is the stiffness matrix due to connection between the beam and tendon at the beam tip via the tip fixture. The detailed expressions can be found in [18,19]. $\mathbf{f} = \mathbf{f}_{ext} + \mathbf{f}_d$ is the force vector, in which $\mathbf{f}_{ext}$ and $\mathbf{f}_d$ are the external and device force vector, respectively.

To derive an approximate equation for the response in the frequency range around the resonance frequency, it is assumed that there is no external force $\mathbf{f}_{ext}$, $\mathbf{f}_d = \mathbf{F}_d\exp(\mathrm{j}\omega t)$ and $\mathbf{q} = \mathbf{Q}\exp(\mathrm{j}\omega t)$. Then, it is convenient to write the dynamic equation Eq. (53) in the following form

$$\big(-\omega^2\mathbf{M} + \mathbf{K}\big)\mathbf{Q} = \mathbf{F}_d \tag{54}$$

Modal analysis is conducted, and the natural circular frequencies ω_i and the corresponding modal vectors $\mathbf{Q}_i$ are determined from the following homogeneous equation of motion

$$\big(\mathbf{K} - \omega_i^2\mathbf{M}\big)\mathbf{Q}_i = \mathbf{0},\ i = 1, 2, \cdots, N \tag{55}$$

where N is the total number of the generalized coordinates.

The relative displacement between the two device ends and the device force vector are expressed, respectively, as

$$q_d = \mathbf{w}(x_d)^{\mathrm{T}}\mathbf{Q},\ \mathbf{F}_d = \mathbf{w}(x_d)F_d \tag{56}$$

where $\mathbf{w}(x) = \begin{bmatrix} \mathbf{W}^{\mathrm{T}}(x) & \mathbf{O} & -\mathbf{W}_t^{\mathrm{T}}(x) & 0 \end{bmatrix}^{\mathrm{T}}$ is the connectivity vector describing the relative motion between the beam and tendon at the location of x, and F_d is the device force. $\mathbf{W}(x)$ and $\mathbf{W}_t(x)$ are the polynomial column vectors used to represent the transverse displacement of the beam and tendon, respectively.

Then the relationship between the relative displacement between the two device ends and the device force is expressed as

$$q_d = \mathbf{w}(x_d)^{\mathrm{T}} \left(-\omega^2 \mathbf{M} + \mathbf{K}\right)^{-1} \mathbf{w}(x_d) F_d \tag{57}$$

It is expanded in terms of the modal frequencies ω_i and the modal vectors $\mathbf{Q}_i$ as follows [23,29]

$$q_d = \sum_{i=1}^{N} \frac{\omega_i^2}{\omega_i^2 - \omega^2} \frac{\left[\mathbf{w}(x_d)^{\mathrm{T}} \mathbf{Q}_i\right]^2}{\mathbf{Q}_i^{\mathrm{T}} \mathbf{K} \mathbf{Q}_i} F_d \tag{58}$$

This equation identifies the modal mass and modal stiffness of i th mode effective for the device location x_d, respectively, as

$$m_i = \frac{\mathbf{Q}_i^{\mathrm{T}} \mathbf{M} \mathbf{Q}_i}{\left[\mathbf{w}(x_d)^{\mathrm{T}} \mathbf{Q}_i\right]^2}, \; k_i = \frac{\mathbf{Q}_i^{\mathrm{T}} \mathbf{K} \mathbf{Q}_i}{\left[\mathbf{w}(x_d)^{\mathrm{T}} \mathbf{Q}_i\right]^2} = \omega_i^2 m_i \tag{59}$$

To increase the damping of a beam-dominated mode with natural frequency of ω_b and modal vector of $\mathbf{Q}_b$, a tendon-dominated mode with natural frequency of ω_t and modal vector of $\mathbf{Q}_t$ is selected for the tuning. The effective modal mass and modal stiffness of the beam-dominated mode are, respectively, given using its modal frequencies ω_b and the modal vectors $\mathbf{Q}_b$ as follows:

$$m_b = \frac{\mathbf{Q}_b^{\mathrm{T}} \mathbf{M} \mathbf{Q}_b}{\left[\mathbf{w}(x_d)^{\mathrm{T}} \mathbf{Q}_b\right]^2}, \; k_b = \omega_b^2 m_b \tag{60}$$

The modal mass of the tendon-dominated mode tends to be much smaller than that of the beam-dominated mode, and it is prone to be influenced by the numerical error and background effect from the other unaccounted modes. Hence, its modal mass here is determined from the fully locked frequency using Eq. (11).

The fully locked frequency can be obtained by assuming an infinitely large device damping. A practical approximation of this conditions is accomplished by introducing a damping matrix as follows:

$$\mathbf{C}_\infty = c_\infty \mathbf{w}(x_d) \mathbf{w}^{\mathrm{T}}(x_d) \tag{61}$$

where c_∞ is a device damping of sufficient high value.

Then, the equation of motion for the beam-tendon system in the fully locked condition is given by

$$\mathbf{M}\ddot{\mathbf{q}} + \mathbf{C}_\infty \dot{\mathbf{q}} + \mathbf{K}\mathbf{q} = \mathbf{0} \tag{62}$$

Modal analysis is conducted, and the fully locked natural circular frequencies $\omega_{\infty i}$ are determined from the following equation

$$\left(-\omega_{\infty i}^2 \mathbf{M} + \mathrm{j}\omega_{\infty i} \mathbf{C}_\infty + \mathbf{K}\right) \mathbf{Q}_{\infty i} = \mathbf{0}, \; i = 1, 2, \cdots, N \tag{63}$$

The corresponding fully locked natural circular frequency ω_∞ is selected from the frequency set $\omega_{\infty i}$. While this frequency does not depend on the stiffness and inertance of the spring-inerter-damper device, it depends on the operating conditions, i.e., the applied axial force, rotational speed, and the device location.

The calibration of the equivalent model is continued by determining the modal mass of the tendon using the fully locked frequency ω_∞ introduced in Eq. (11) and the knowledge of the targeted subsystem frequencies as follows:

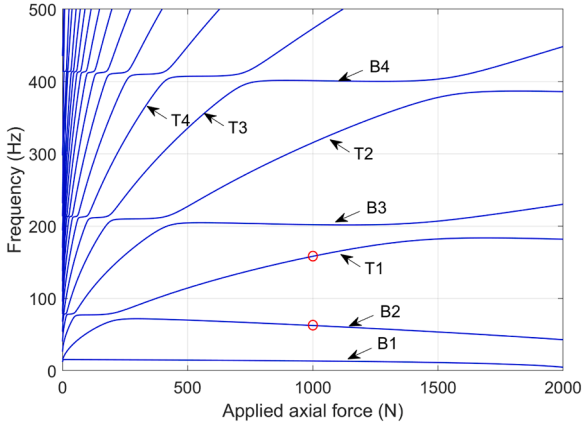

Fig. 10. The change of the natural frequencies with increasing applied axial force P when the rotational speed is 45 rad/s for the beam-tendon system with no device. The frequencies denoted by the red circles indicate the frequencies for B2 and T1 modes in the operating condition.

$$m_t = m_b \frac{\omega_b^2 - \omega_\infty^2}{\omega_\infty^2 - \omega_t^2} \tag{64}$$

After this, the modal stiffness of the tendon-dominated mode is determined using its natural frequency and previously obtained modal mass m_t as follows:

$$k_t = \omega_t^2 m_t \tag{65}$$

Having the modal masses and stiffnesses corresponding to the considered beam and tendon-dominated mode pair determined, for a given spring-inerter-damper device placed at the location of x_d shown in Fig. 9, the minimum 2DOF system shown in Fig. 2 is adopted to approximately represent the full-scale beam-tendon system. The results and conclusions achieved using the 2DOF reduced order surrogate representation thus can help to elucidate the observations made during the full-scale beam-tendon analysis. For instance, the parameters corresponding to the optimal tuning condition can be calculated according to Table 2.

3.2. Case study

This subsection presents the case study involving the design of the parameters of the device based on the equivalent 2DOF system and their comparison with the full-scale optimal design. Firstly, in the reference operating condition, the coupling device stiffness is fixed while the inertance for the optimal tuning is determined according to the equivalent 2DOF system results. Then, the device inertance is fixed while determining the optimal device stiffness. After this, the system performance is evaluated in other operating conditions. The applied axial force is 1000 N and the rotational speed is 45 rad/s in the reference operating condition. The device is located at $0.6L$. The change of the natural frequencies with the increasing applied axial force P when the rotational speed is 45 rad/s for the system with no device is illustrated in Fig. 10. The label Bx marks the x-th beam-dominated mode, while Tx stands for the x-th tendon-dominated mode. The frequencies of the beam-dominated modes (B1-B4) decrease slightly with the increasing axial force, while the frequencies of the tendon-dominated modes (T1-T4) increase rapidly with the increasing axial force. The curve veering takes place when one frequency locus approaches the other with the increasing force due to dynamic coupling [32]. The objective is to tune the second beam-dominated mode B2 using the first tendon-dominated mode T1 when the axial force P is 1000 N, as indicated by the red circles in Fig. 10. In the reference operating condition, the modal mass and stiffness of these two modes in the equivalent 2DOF system are provided in Table 3.

The following subsections compare the full-scale system with the device parameters determined from the equivalent 2DOF system and the full-scale system with the optimal device parameters in the cases of the fixed device stiffness and fixed device inertance.

3.2.1. Fixed device stiffness

When the device stiffness is fixed, the device inertance (b_*), the device damping (c_{b1}) and damping ratio (ζ_{b1}) at the first bifurcation point, as well as the device damping at the second bifurcation point (c_{b2*}) in the optimal tuning condition are determined through the equivalent 2DOF system and are listed in Table 4. The corresponding full-scale optimal parameters are determined by trial and error and are also listed in the Table 4 for comparison. The differences between the two parameter sets are calculated and shown in Table 4 as well. It can be seen that the equivalent 2DOF system gives very accurate estimates of the optimal parameters for the beam-tendon system with errors less than 5 % for a range of different device stiffness. It can further be seen that when the device stiffness is increased, the required device inertance for optimal tuning is increased, and the required device damping at the first bifurcation point (c_{b1}) and the second bifurcation point are also increased. However, the damping ratio at the first bifurcation point (ζ_{b1}) is reduced, which is consistent with the conclusion in Section 2.2.3. To increase the damping ratio of the targeted mode optimally, it is desirable to increase this damping ratio, so increasing device stiffness is not beneficial for the system performance in this case.

For the above reason, the variation of the damped natural frequencies and damping ratios with the increasing device damping at the selected device inertances when the device stiffness is 0 N/m is plotted in Fig. 11. With the increase of the device inertance, the system changes from the subcritical condition to the supercritical condition, which is consistent with the analyses for the 2DOF system in Section 2.3.1. In addition, it can be seen that the damping ratio at the first bifurcation point in the optimal tuning plane is larger than the maximum damping ratio for the localised loci in any other planes.

A comparison of the frequency loci in the complex plane obtained when increasing the device damping c between three different cases when the device stiffness is 0 N/m is given in Fig. 12. One case represents the optimal tuned system for the full-scale continuous beam-tendon system (device inertance is 0.0092 kg); the second case is the full-scale continuous system which uses the device

Table 3
The parameters of the equivalent 2DOF system of the beam-tendon system in the reference operating condition.

Parameters	Values
m_b	0.0519 kg
k_b	7967.36 N/m
m_t	0.005 kg
k_t	4961.83 N/m

Table 4
The comparison of the parameters determined from the equivalent 2DOF system and the optimal continuous system for different device stiffness conditions.

System*	Stiffness k_* (N/m)	b_* (kg)	c_{b1} (Ns/m)	ζ_{b1}	c_{b2*}(Ns/m)
2DOF	0	0.0089	7.79	0.3037	14.01
optimal		0.0092	7.75	0.3032	13.38
error		3.2 %	<1 %	<1 %	4.7 %
2DOF	10^3	0.0133	8.98	0.2636	18.21
optimal		0.0136	8.95	0.2679	17.55
error		2.2 %	<1 %	1.6 %	3.8 %
2DOF	10^4	0.0529	16.10	0.1469	55.97
optimal		0.05319	16.15	0.1480	55.30
error		<1 %	<1 %	<1 %	1.2 %
2DOF	10^5	0.4489	45.23	0.0523	433.56
optimal		0.44924	45.48	0.0527	432.90
error		<1 %	<1 %	<1 %	<1 %

* '2DOF' means the parameters are calculated using the equivalent 2DOF system, 'optimal' means the parameters are the optimal ones for the full-scale coupled beam-tendon system.

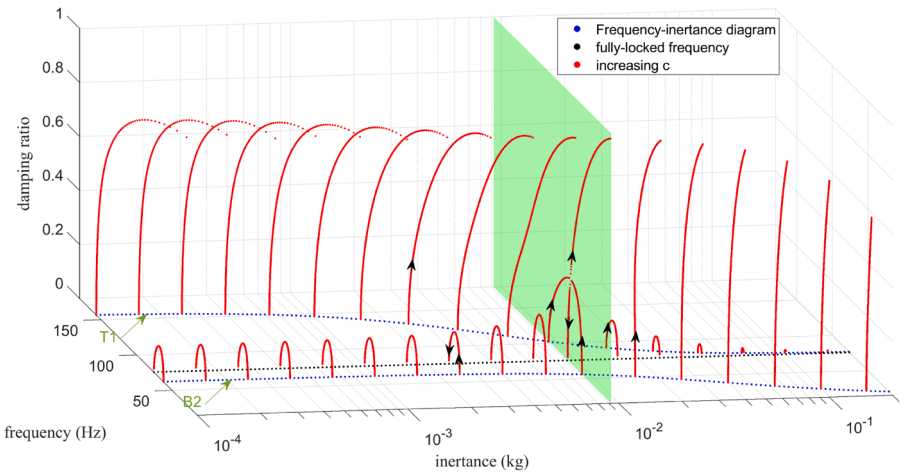

Fig. 11. The variation of the damped natural frequencies and damping ratios with the increasing device damping at the selected device inertances when the device stiffness is 0. Blue: the frequency-inertance diagram for the undamped system; black: the locus of the fully locked frequency with inertance; red: the damped frequency-damping ratio loci at the selected inertances. The arrows denote the direction of increasing device damping c. The green plane is the optimal tuning plane.

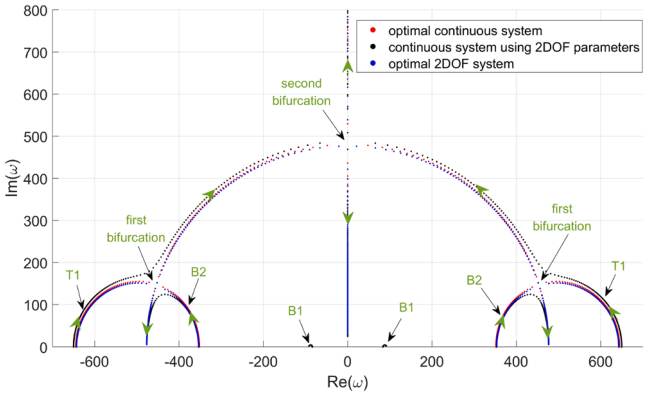

Fig. 12. The comparison of the root loci in the complex plane obtained when increasing the device damping c between the three cases when the device stiffness is 0 N/m. 'Optimal continuous system' represents the optimal tuning case for the continuous beam-tendon system (device inertance is 0.0092 kg); 'continuous system using 2DOF parameters' represents the continuous system adopting the device parameters determined through the equivalent 2DOF model (device inertance is 0.0089 kg); 'optimal 2DOF system' represents the optimal tuning for the equivalent 2DOF model (device inertance is 0.0089 kg). The arrows represent the direction of increasing device damping c.

parameters determined through the equivalent 2DOF system (device inertance is 0.0089 kg); and the third case is the optimal tuned equivalent 2DOF system (device inertance is 0.0089 kg). It can be seen that the loci for the optimal continuous system are almost identical to the optimal equivalent 2DOF system. This confirms that the continuous beam-tendon system can be effectively reduced to an equivalent 2DOF system discussed previously when studying the dynamic interactions between the two reference subsystem-dominated modes. The loci of the full-scale continuous system computed using the 2DOF parameters are very close to the two other cases. Although there is no significant difference between the determined device inertances (error 3.2 %), owing to the sensitivity of the optimal tuning condition to this parameter, this system does not reach the fully optimal tuning condition.

To compare the performance between the optimal continuous system and the continuous system using the 2DOF parameters when the device operates at the first bifurcation point, the driving-point receptances at the beam tip are calculated and shown in Fig. 13. To achieve this, the force F is applied at the beam tip (shown in Fig. 9) and the frequency response function from the force F to the beam tip displacement is calculated using the corresponding equation given in [19]. Compared to the reference system with no device, these two systems suppress the B2 mode significantly. This is because the frequencies of the targeted B2 and T1 modes become very close and both damping ratios attain high values. The device increases the damping ratios of other beam-dominated modes slightly, e.g., B1 and B3 modes. The T2 mode disappears from the considered frequency range because the device reduces the effective length of the tendon, hence all tendon-dominated frequencies are increased [19]. Although the continuous system which uses the 2DOF parameters does not reach the fully optimal tuning condition, its receptance does not show significant difference from that of the optimal continuous system. This means the device parameters determined from the equivalent 2DOF system can be adopted and used in the continuous system to get a system performance close to the optimal performance.

3.2.2. *Fixed device inertance*

When the device inertance is fixed, the device stiffness (k_*), the device damping (c_{b1}) and damping ratio (ζ_{b1}) at the first bifurcation point, as well as the device damping at the second bifurcation point (c_{b2*}) in the optimal tuning condition, determined using the equivalent 2DOF system, are all listed in Table 5. The corresponding full-scale model optimal parameters and the resulting differences are also listed in the table. The equivalent 2DOF system gives very accurate estimation of the optimal parameters for the beam-tendon system with errors less than 6 % across the different device inertance conditions. It can be seen that when the device inertance is increased, the required device stiffness for optimal tuning, the required device damping at the first bifurcation point (c_{b1}) as well as at the second bifurcation point are also increased. However, the damping ratio at the first bifurcation point (ζ_{b1}) is reduced, which is consistent with the conclusion in Section 2.2.3. To increase the damping ratio of the targeted mode optimally, it is desirable to increase this damping ratio, hence increasing the device inertance is not beneficial for the system performance in this case.

The variation of the damped natural frequencies and damping ratios with the increasing device damping at the selected device stiffness when the device inertance is 0.015 kg is plotted in Fig. 14. With the increase of the device stiffness, the system changes from supercritical condition to subcritical condition, which is consistent with the analyses for the 2DOF system in Section 2.3.2. In addition, the damping ratio at the first bifurcation point in the optimal tuning plane is larger than the maximum damping ratio for the localised loci in any other planes.

A comparison of the frequency loci in the complex plane obtained when increasing the device damping c between three systems when the device inertance is 0.015 kg is illustrated in Fig. 15. It can be seen that the loci for the optimal continuous system are almost identical to the optimal equivalent 2DOF system, which still confirms that the continuous beam-tendon system when considering two coupled modes can be reduced to 2DOF system. The loci for the continuous system using 2DOF parameters are very close to the above two, although the system does not reach the optimal tuning condition. The optimal tuning plane is very sensitive to the device stiffness,

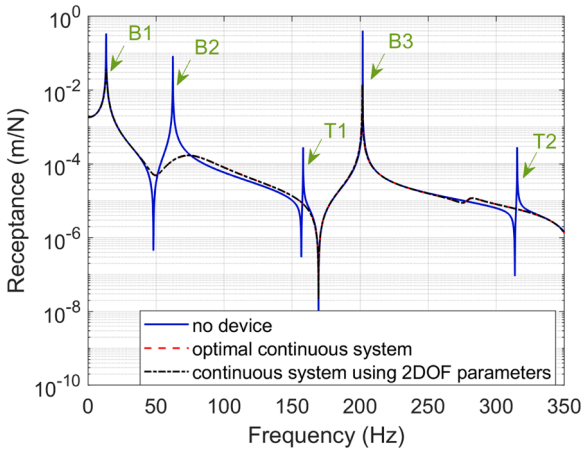

Fig. 13. The comparison of the driving-point receptances at the beam tip between three cases when the device stiffness is 0 N/m. 'no device' represents the beam-tendon system with no device; 'optimal continuous system' represents the optimal tuning for the continuous beam-tendon system (device inertance is 0.0092 kg, device damping is 7.75 Ns/m); 'continuous system using 2DOF parameters' represents the continuous system using the device parameters determined through the equivalent 2DOF system (device inertance is 0.0089 kg, device damping is 7.79 Ns/m).

Table 5
The comparison of the parameters determined from the equivalent 2DOF system and the optimal continuous system for different device inertance conditions.

System*	Inertance b_* (kg)	k_* (N/m)	c_{b1} (Ns/m)	ζ_{b1}	c_{b2*}(Ns/m)
2DOF	0.015	1393.1	9.40	0.2517	19.86
optimal		1318	9.30	0.2565	18.89
error		5.7 %	1.1 %	1.9 %	5.1 %
2DOF	0.05	9346.6	15.69	0.1508	53.23
optimal		9275	15.70	0.1508	52.28
error		<1 %	<1 %	<1 %	1.8 %
2DOF	0.10	20,709	21.72	0.1089	100.90
optimal		20,637	21.78	0.110	99.95
error		<1 %	<1 %	1.0 %	1.0 %
2DOF	0.30	66,157	37.07	0.0638	291.58
optimal		66,085	37.25	0.0637	290.65
error		<1 %	<1 %	<1 %	<1 %

* '2DOF' means the parameters are calculated using the equivalent 2DOF system, 'optimal' means the parameters are the optimal ones for the full scale coupled beam-tendon system.

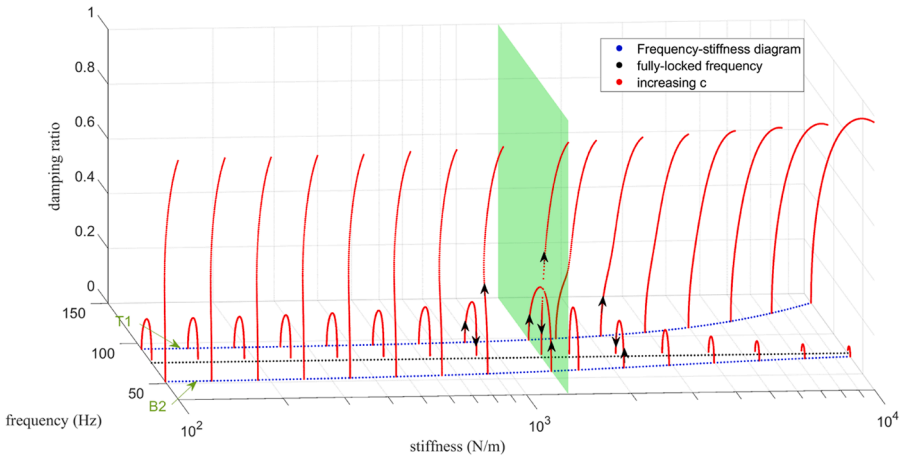

Fig. 14. The variation of the damped natural frequencies and damping ratios with the increasing device damping at the selected device stiffness values when the device inertance is 0.015 kg. Blue: the frequency-stiffness diagram for the undamped system; black: the change of the fully locked frequency with the stiffness; red: the damped frequency-damping ratio loci at the selected stiffness values. The arrows denote the direction of increasing device damping c. The green plane is the optimal tuning plane.

although there is no much difference between the device stiffness (error 5.7 %).

The driving-point receptances at the beam tip are plotted in Fig. 16 to compare the performance between the optimal continuous system and the continuous system which uses the 2DOF parameters when the device operates at the first bifurcation point. Compared to the system with no device, these two systems demonstrate significant increase in damping of B2 mode. The increase in the damping ratios of the other beam-dominated modes, e.g., B1 and B3, is slight. Although the continuous system which uses the 2DOF parameters does not reach the fully optimal tuning condition, its receptance does not show significant difference from the optimal continuous system. It means the device parameters determined from the equivalent 2DOF system can be used in the continuous system to reach the near-optimal performance.

3.2.3. System performance

The objective of designing the spring-inerter-damper device is to increase the damping of the targeted beam-dominated modes in the wide ranges of the axial forces and rotational speeds. This will be important in future rotorcraft applications where the rotational speed of the blades may vary while the adjustable axial forces could be introduced to ensure resonance avoidance. Thus, the motivation of this subsection is to evaluate the system performance in wide ranges of the applied axial force and rotational speeds.

The device parameters are determined from the equivalent 2DOF system in the reference operating condition of the axial force 1000 N and rotational speed 45 rad/s. This leads to the device stiffness 0 N/m, device inertance 0.0089 kg, and device damping 7.79 Ns/m. These device parameters are selected because the corresponding damping ratio (0.3037) at the first bifurcation is the largest. Next, the driving-point receptances at the beam tip are compared between the beam-tendon system with no device and the above system with the device parameters determined from the equivalent 2DOF systems for a range of different applied axial forces (Fig. 17a) and different rotational speeds (Fig. 17b). Although the device parameters are determined for the reference axial force of 1000 N, the

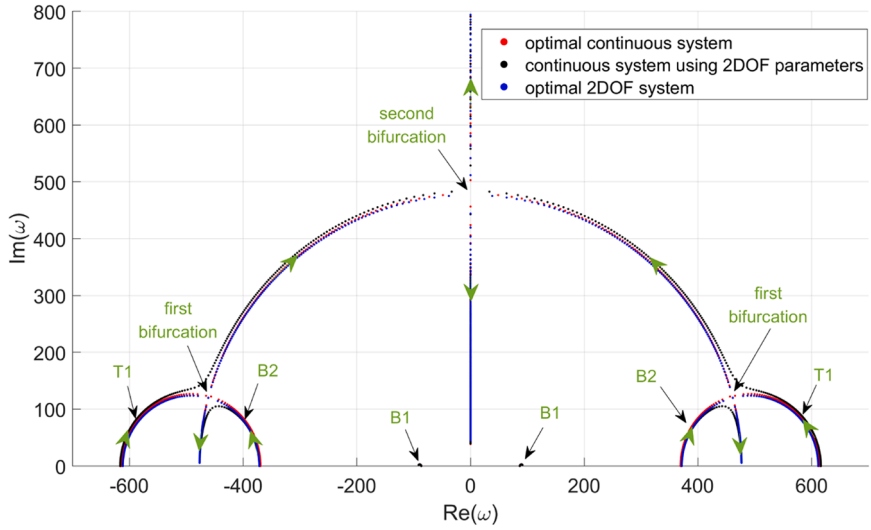

Fig. 15. The comparison of the root loci in the complex plane obtained when increasing the device damping c between the three systems when the device inertance is 0.015 kg. 'Optimal continuous system' represents the optimal tuning for the continuous beam-tendon system (device stiffness is 1318 N/m); 'continuous system using 2DOF parameters' represents the continuous system using the device parameters determined through the equivalent 2DOF system (device stiffness is 1393.1 N/m); 'optimal 2DOF system' means the optimal tuning for the equivalent 2DOF system (device stiffness is 1393.1 N/m). The arrows represent the direction of increasing device damping c.

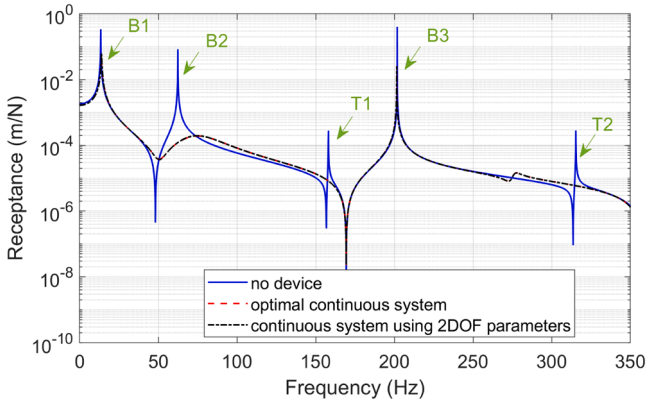

Fig. 16. The comparison of the driving-point receptances at the beam tip between the three systems when the device inertance is 0.015 kg. 'no device' represents the beam-tendon system with no device; 'optimal continuous system' represents the optimal tuning for the continuous beam-tendon system (device stiffness is 1318 N/m, device damping is 9.30 Ns/m); 'continuous system using 2DOF parameters' represents the continuous system using the device parameters determined through the equivalent 2DOF system (device stiffness is 1393.1 N/m, device damping is 9.40 Ns/m).

device can reasonably suppress the B2 mode in the wide range of the axial forces, e.g., between 400 N and 1900 N. It is observed that the resulting effect is better under the higher axial forces. This is because the damping ratio of the beam-dominated mode increases with the increasing axial force when the device damping is fixed [19]. Although the device parameters are determined for the rotational speed of 45 rad/s, the device can suppress B2 mode effectively in a wide range of the rotational speeds, e.g., between 5 rad/s and 85 rad/s. These results show that when the device parameters are designed for a certain reference operating condition, they can be used effectively in other operating conditions. This outcome shows the broad applicability of the device in the rotating beam-tendon systems undergoing wide parametric or operational changes.

4. Discussion

This paper proposes a new computationally efficient method to design the optimal device parameters for a continuous system through the equivalent 2DOF system. This approach makes the calculation of the device parameters efficient and straightforward. A different method based on the optimization of the full-scale problem was proposed by the authors in a previous study [19]. The original

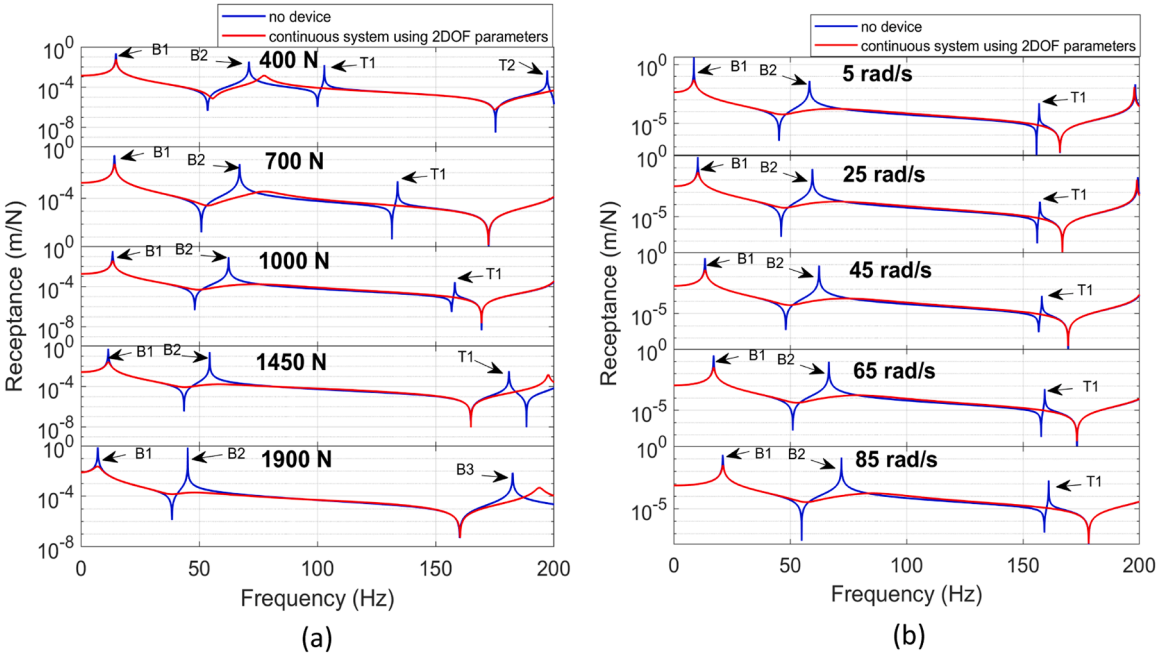

Fig. 17. The comparison of the driving-point receptances between the beam-tendon system with no device and the system with the device parameters determined from the equivalent 2DOF system (device stiffness is 0 N/m, device inertance is 0.0089 kg, device damping is 7.79 Ns/m): (a) under different applied axial forces, (b) under different rotational speeds.

optimization-based method derived the device inertance or stiffness based on Eq. (16) which used the relationship between the two undamped frequencies and the fully locked frequency. The device damping was derived based on the fact that the two roots at the first bifurcation in the optimal tuning condition were the same. This optimization-based method was applied to a rotating beam-tendon

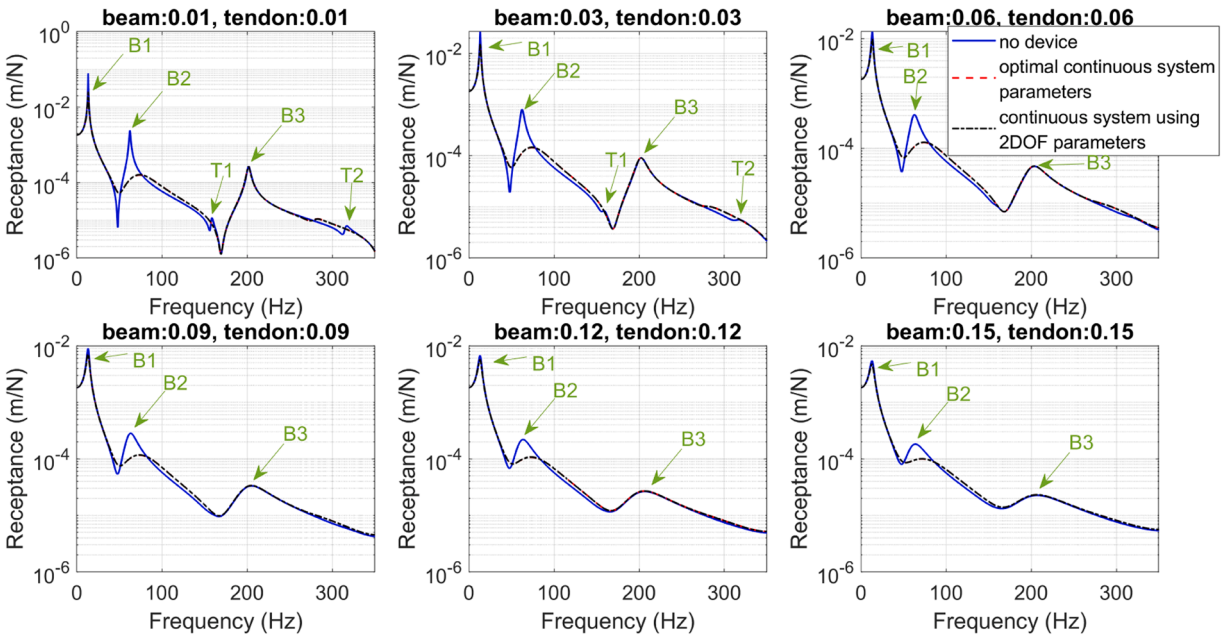

Fig. 18. The comparison of the driving-point receptances at the beam tip between three cases when the device stiffness is 0 N/m and different levels of damping ratios for the beam and tendon are considered. 'no device' represents the beam-tendon system with no device; 'optimal continuous system parameters' represents using the device parameters for the optimal tuning of the continuous beam-tendon system with no structural damping (device inertance is 0.0092 kg, device damping is 7.75 Ns/m); 'continuous system using 2DOF parameters' represents the continuous system using the device parameters determined through the equivalent 2DOF system (device inertance is 0.0089 kg, device damping is 7.79 Ns/m).

system in [19] and another rotating blade-tendon system in [36] to design the optimal device parameters. However, that method was characterised by a significant computational penalty and a substantially less straightforward process of arriving at the optimal set of the device parameters. In addition, the new method proposed in this paper establishes a solid theoretical bridge between the continuous system and its equivalent 2DOF representation, which helps us to understand and design the continuous system from the perspective of its equivalent 2DOF system.

The design method presented in this paper is based on method 3 described in Section 1. The suitability of each of the reviewed methods depends on the specific context. Krenk [22] compared the effectiveness of these three methods when studying a 1DOF system equipped with the tuned mass damper. It was found that the frequency tuning was the same for these three methods. The device damping for method 1 was the lowest, followed by method 2, and finally by method 3. In terms of the structural mass response in the frequency domain, it was found to be flat when using method 2, while it featured a trough when using method 1 and a single peak when using method 3. However, in terms of the relative motion between the masses, method 1 produced two distinct peaks, method 2 led to a wide and flat peak, and method 3 to a narrow peak. Hence, methods 2 or 3 could be favoured in the test case. Later, method 2 was applied to a case study involving a flexible structure [23]. For the current application consisting of two coupled subsystems, the aim was to effectively activate the spring-inerter-damper device through increased subsystem coupling. Method 3 was used to develop the tuning strategy. Given the targeted application context, this choice was made due to its greater analytical tractability compared to the two other methods as well as due to its close relationship to the inherent dynamic characteristics of the studied problem. Following the approach in method 3, the expected dynamic behaviour was stimulated by tuning the combined system such that there was no separation between the two subsystem frequencies and the damping ratios for both subsystems acquired the same level. It should be noted that the damping ratios of both systems do not reach their maxima at the first bifurcation point in method 3, but it is sufficient for application. If the results in [22] are also applicable to the system in this paper, then it is obvious that methods 1 and 2 require smaller device damping, and they correspond to the case when the device damping $c \leq c_{b1}$ (the system before the first bifurcation) in Section 2.2.4. So the two subsystems have the same damping ratios but there is separation between their frequencies. Featuring certain frequency separation, this case can still lead to the unfavourable presence of the two distinct resonant peaks.

In the equivalent 2DOF system, the inherent damping of the two subsystems is not considered. This is based on the fact that the baseline mechanical structure usually has low structural damping (e.g., damping ratio <0.05), which, ultimately, is the main reason for introducing additional sources of energy dissipation. However, it is expected that the results derived from the undamped equivalent 2DOF system will still be applicable to the weakly damped 2DOF and continuous systems. For example, as shown in Fig. 18, when different levels of modal damping ratios of the beam and tendon are considered, increasing from 0.01 to 0.15, the driving-point receptances at the beam tip are compared between three cases. The modal damping ratios are added by adding a damping matrix using the method in [18]. The device parameters are the same as those obtained when no structural damping is considered, as in Fig. 13. The tendon modes (T1, T2) become concealed with increasing damping ratio. The targeted B2 mode is suppressed significantly in all 6 cases. The response of the system using optimal continuous system parameters is almost identical to that of the continuous system which uses the device parameters determined through the equivalent 2DOF system. This result confirms the above suggestion. This approach is also supported by the previous studies [19,36] which did take into consideration the structural damping of the investigated beam and blade structures.

In this paper, the effective modal mass and stiffness of the primary continuous system are derived based on the correction of the much smaller modal mass of one subsystem using Eq. (11). It was found that if no correction was applied, the derived device parameters were far from being optimal. Hence, this corrective measure is deemed necessary. The comparisons presented in Section 3.2 demonstrate that the device parameters derived using the corrected equivalent system are very close to the optimal parameters (errors usually within 6 %) and the resulting system performance is almost identical to the optimal performance determined using the full-scale continuous system. It is recommended that the subsystem with the smaller modal mass is corrected since it is prone to be influenced by the numerical errors and background effects from other neighbouring modes. However, a drawback of this approach is that the fully locked frequency is needed to implement the correction. To derive the modal mass and stiffness directly from the original system or to correct the device parameters, Krenk's quasi-dynamic flexibility and inertia corrections [29] may be considered. Krenk [29] provides a method that takes into account the background effect from the non-resonant modes through adding a stiffness term and an inertia term directly.

As introduced in the Introduction, the paper fits in the framework of advancing the active tendon concept for the resonance avoidance – primarily in the context of the helicopter blades [20]. This study addresses the problem of how to design the spring-inerter-damper device parameters for optimal vibration suppression. Therefore, this study further promotes the active tendon concept to its practical application in the rotors undergoing configurational or operational changes.

5. Conclusion

The motivation behind this work is the problem of finding the optimal parameters for a spring-inerter-damper device linking the two flexible subsystems such that optimum passive vibration control is achieved. To address this problem efficiently, a minimum dynamic equivalence is proposed in the form of a 2DOF system, and comprehensive and systematic mathematical analyses are carried out for the 2DOF system. Then, the equivalence between the 2DOF system and the full-scale continuous system is established, which allows the results of the 2DOF system to be directly transferrable to the original full-scale system. Some conclusions and results of the study are summarized as follows:

(1) By studying the 2DOF system, it is found that there is an optimal tuning condition in which the two roots coalesce and both damping ratios share optimally balanced large value at the first bifurcation point. The device parameters in this condition are derived analytically, including the critical device inertance and stiffness as well as the damping at the first and second bifurcation points. It is shown that the increase in the device inertance or stiffness causes decrease in the achievable optimal damping ratio at the first bifurcation point. In the optimal tuning plane, before the first bifurcation, the damping ratios of the four roots are the same, while the multiplication of the moduli of two roots on the same side is a constant; Between the first and second bifurcation, the moduli of the four roots are the same, while the multiplication of the damping ratios of two roots on the same side is a constant; After the second bifurcation, two roots become purely imaginary and the multiplication of these moduli is a constant, while the other two complex roots are still on the circle of a radius equal to the fully locked frequency.
(2) The subcritical and supercritical conditions are defined. The subcritical condition, featuring that the non-local loci encompass the local loci, is reached when the device inertance is less than the critical inertance, or when the device stiffness is larger than the critical stiffness. The supercritical condition, featuring that the local loci locate outside the non-local loci, is reached when the device inertance is larger than the critical inertance, or when the device stiffness is less than the critical stiffness. There are three properties for subcritical and supercritical complex root planes, i.e., (1) The non-local and local trajectories will never cross in the subcritical and supercritical planes; (2) The loci with larger undamped frequency is non-local in the subcritical plane, while the loci with smaller undamped frequency is non-local in the supercritical plane; (3) The local and non-local trajectories are always separated by the fully locked frequency before the second bifurcation in both the subcritical and supercritical planes.
(3) A procedure for determining the equivalent lumped parameter 2DOF system for continuous systems is proposed in order to apply the results of the 2DOF analysis directly to these continuous systems. To assess its performance and demonstrate its application, a case study of a rotating beam-tendon system is conducted. A coupling device is used to internally connect the beam and tendon to suppress the resonance of a targeted beam-dominated mode. The device parameters derived based on the equivalent 2DOF system are shown to be close to the optimal parameters with errors less than 6 %. The resulting full-scale system performance adopting the 2DOF optimal device parameters is shown to be almost identical to the optimal performance. Further, the derived device parameters allow the beam-tendon system to perform well not only in the reference operating condition but also in wide ranges of axial force and rotational speed.

This study further advances the understanding of the active tendon concept toward its practical application in the rotors undergoing configurational or operational changes.

CRediT authorship contribution statement

Jun Wu: Writing – review & editing, Writing – original draft, Validation, Software, Methodology, Investigation, Formal analysis, Conceptualization. **Brano Titurus:** Writing – review & editing, Methodology, Conceptualization.

Declaration of competing interest

The authors declare that they have no known competing financial interests or personal relationships that could have appeared to influence the work reported in this paper.

References

[1] S. Krenk, S.R. Nielsen, Vibrations of a shallow cable with a viscous damper, Proc. R. Soc. Lond. 458 (2002) 339–357. Series A: Mathematical, Physical and Engineering Sciences.
[2] B.M. Pacheco, Y. Fujino, A. Sulekh, Estimation curve for modal damping in stay cables with viscous damper, J. Struct. Eng. 119 (1993) 1961–1979.
[3] S. Krenk, Vibrations of a taut cable with an external damper, J. Appl. Mech. 67 (2000) 772–776.
[4] J.A. Main, N.P. Jones, Free vibrations of taut cable with attached damper. I: linear viscous damper, J. Eng. Mech. 128 (2002) 1062–1071.
[5] J.A. Main, N.P. Jones, Vibration of tensioned beams with intermediate damper. I: formulation, influence of damper location, J. Eng. Mech. 133 (2007) 369–378.
[6] J.A. Main, N.P. Jones, Vibration of tensioned beams with intermediate damper. II: damper near a support, J. Eng. Mech. 133 (2007) 379–388.
[7] L. Lu, Y.-F. Duan, B.F. Spencer, X. Lu, Y. Zhou, Inertial mass damper for mitigating cable vibration, Struct. Control Health Monit. 24 (2017).
[8] J. Ormondroyd, J.P.D. Hartog, The theory of the dynamic vibration absorber, J. Fluids. Eng. 49 (1928).
[9] G.M. Stewart, M.A. Lackner, The impact of passive tuned mass dampers and wind–wave misalignment on offshore wind turbine loads, Eng. Struct. 73 (2014) 54–61.
[10] L. Byers, F. Gandhi, Embedded absorbers for helicopter rotor lag damping, J. Sound. Vib. 325 (2009) 705–721.
[11] D. Han, E.C. Smith, Lagwise loads analysis of a rotor blade with an embedded chordwise absorber, J. Aircr. 46 (2009) 1280–1290.
[12] J. Austruy, F. Gandhi, N. Lieven, Rotor vibration reduction using an embedded spanwise absorber, J. Am. Helicopter Soc. 57 (2012) 49–60.
[13] H.N. Özgüven, B. Candir, Suppressing the first and second resonances of beams by dynamic vibration absorbers, J. Sound. Vib. 111 (1986) 377–390.
[14] R.G. Jacquot, Optimal dynamic vibration absorbers for general beam systems, J. Sound. Vib. 60 (1978) 535–542.
[15] L. Sun, D. Hong, L. Chen, Cables interconnected with tuned inerter damper for vibration mitigation, Eng. Struct. 151 (2017) 57–67.
[16] C.P. Szczyglowski, S.A. Neild, B. Titurus, J.Z. Jiang, E. Coetzee, Passive gust loads alleviation in a truss-braced wing using an inerter-based device, J. Aircr. 56 (2019) 2260–2271.
[17] A.d.S. Pippi, S.M. Avila, G. Doz, A review on the use of the inerter device in the structural coupling technique for adjacent building vibration control, Structures 42 (2022) 480–501.
[18] J. Wu, B. Titurus, Damping augmentation of a rotating beam-tendon system via internally placed spring-damper elements, J. Sound. Vib. 510 (2021).
[19] J. Wu, B. Titurus, Vibration control of a rotating Timoshenko beam-tendon system via internal guiding inerter-dampers, J. Sound. Vib. 516 (2022).
[20] J. Rauleder, B.G. van der Wall, A. Abdelmoula, D. Komp, S. Kumar, V. Ondra, B. Titurus, B.K. Woods, Aerodynamic performance of morphing blades and rotor systems, in: Proceedings of the AHS International 74th Annual Forum & Technology Display, Phoenix, Arizona, USA, 2018.
[21] J.P.D. Hartog, Mechanical Vibrations, McGraw-Hill Book Company, New York, 1985.

[22] S. Krenk, Frequency analysis of the tuned mass damper, J. Appl. Mech. 72 (2005) 936–942.
[23] S. Krenk, J. Høgsberg, Tuned mass absorber on a flexible structure, J. Sound. Vib. 333 (2014) 1577–1595.
[24] Z. Zhang, X. Li, B. Chen, X. Hua, Closed-form optimal design of the tuned inerter damper (TID) connecting adjacent flexible buildings, Eng. Struct. 302 (2024).
[25] N. Alujević, D. Čakmak, H. Wolf, M. Jokić, Passive and active vibration isolation systems using inerter, J. Sound. Vib. 418 (2018) 163–183.
[26] M. Basili, M. De Angelis, D. Pietrosanti, Modal analysis and dynamic response of two adjacent single-degree-of-freedom systems linked by spring-dashpot-inerter elements, Eng. Struct. 174 (2018) 736–752.
[27] M. Basili, M. De Angelis, D. Pietrosanti, Defective two adjacent single degree of freedom systems linked by spring-dashpot-inerter for vibration control, Eng. Struct. 188 (2019) 480–492.
[28] J. Song, K. Bi, R. Ma, Z. Wang, K. Xu, H. Hao, Vibration control of adjacent structures equipped with inerter-based dampers considering nonlinearities: analytical and experimental studies, Mech. Syst. Signal. Process. 206 (2024).
[29] S. Krenk, J. Høgsberg, Tuned resonant mass or inerter-based absorbers: unified calibration with quasi-dynamic flexibility and inertia correction, Proc. R. Soc. A Math. Phys. Eng. Sci. 472 (2016).
[30] S. Krenk, Resonant inerter based vibration absorbers on flexible structures, J. Franklin. Inst. 356 (2019) 7704–7730.
[31] J. Wu, V. Ondra, J. Luebker, S. Kalow, J. Riemenschneider, B. Titurus, Experimental modal analysis of a rotating tendon-loaded helicopter blade demonstrator, Mech. Syst. Signal. Process. 178 (2022).
[32] V. Ondra, B. Titurus, Theoretical and experimental modal analysis of a beam-tendon system, Mech. Syst. Signal. Process. 132 (2019) 55–71.
[33] V. Ondra, B. Titurus, Free vibration analysis of a rotating pre-twisted beam subjected to tendon-induced axial loading, J. Sound. Vib. 461 (2019).
[34] J. Wu, B. Titurus, Modal analysis of a rotating pre-twisted beam axially loaded by an internally guided tendon, J. Sound. Vib. 498 (2021).
[35] V. Ondra, B. Titurus, Free vibration and stability analysis of a cantilever beam axially loaded by an intermittently attached tendon, Mech. Syst. Signal. Process. 158 (2020).
[36] S. Jayatilake, J. Wu, B. Titurus, Tendon-inerter-damper helicopter blade augmentation for improved dynamic performance, J. Sound. Vib. 547 (2023).